The characteristics of synaptic vesicle dynamics at hippocampal mossy fiber terminals

Rinako Miyano

Graduate School of Brain Science, Doshisha University

A thesis submitted for the degree of
Doctor of Philosophy in Science
March 2023

Abstract

Hippocampal mossy fiber terminals are one of the cortical terminals, which are sufficiently large to be accessible by patch-clamp technique. At presynaptic terminals, Ca^{2+} potentially controls the amounts of neurotransmitter release by acting on multiple steps of vesicle cycling, thereby inducing short- and long-term synaptic plasticity (Zucker & Regehr, 2002). These steps include synaptic vesicle recruitment, docking, priming, fusion, and endocytosis. To measure the Ca^{2+}-dependence of exo- and endocytotic kinetics quantitatively, I applied presynaptic capacitance measurements to the mossy fiber terminal of acute brain slices at room temperature. In the first part, I have characterized the basic properties of synaptic vesicle exocytosis and endocytosis. The time course of synaptic vesicle fusion was slow, with a time constant of tens of milliseconds. At calyx of Held synapses having high release probability, neurotransmitter release is fast with a release time constant of a few milliseconds. Comparison of the release time course with hippocampal mossy fiber terminals suggests that mossy fiber synapses have synaptic vesicles with low release probability. The release was sensitive to Ca^{2+} buffers EGTA and BAPTA, suggesting a loose coupling between Ca^{2+} channels and synaptic vesicles. The size of the readily releasable pool (RRP) of synaptic vesicles was insensitive to Ca^{2+} buffers. Once the RRP was depleted, it was recovered by a single exponential with a time constant of ~1 s independent of the presence of Ca^{2+} buffers, suggesting Ca^{2+}-independent vesicle replenishment. In addition to the RRP, the reserve pool (RP) of vesicles was released slowly

during repetitive stimulation. Endocytosis was also insensitive to Ca^{2+} buffers and had a slow time course, excluding the involvement of rapid vesicle cycling in vesicle replenishment. Although mossy fiber terminals are known to have various forms of Ca^{2+}-dependent plasticity, some features of vesicle dynamics are robust and Ca^{2+}-insensitive. A large vesicle pool and low release probability due to loose coupling between Ca^{2+} channels and synaptic vesicles may allow dynamic changes of synaptic strength during short- and long-term potentiation by increasing release probability.

In the second part, I have addressed the molecular mechanisms of synaptic vesicle exocytosis by combining electrophysiology and genetics. Synaptic vesicles dock and fuse at the presynaptic active zone (AZ), the specialized site for transmitter release. AZ proteins play multiple roles such as recruitment of Ca^{2+} channels as well as synaptic vesicle docking, priming and fusion. Rab3-interacting molecule-binding protein 2 (RIM-BP2) is one of the AZ-scaffold proteins and interacts with Ca^{2+} channels and synaptic vesicles. However, compared to other AZ-scaffold proteins, functional roles of RIM-BP2 are less known. Revealing the roles of RIM-BP2 in neurotransmitter release may contribute to an understanding of molecular mechanisms of synaptic transmission and synaptic plasticity. At phasic synapses having high release probability, RIM-BP2 is known to affect Ca^{2+} channel localization at AZs. In order to dissect the role of RIM-BP2 at tonic synapses having low release probability, I applied electrophysiological recording and super-resolution imaging to hippocampal mossy fiber terminals of RIM-BP2 KO mice. By using whole cell capacitance measurements, I found that reduced Ca^{2+} currents were responsible for the decreased rates of

transmitter release in RIM-BP2 KO terminals. Consistently, STED microscopy confirmed lower densities of P/Q-type Ca^{2+} channels at AZs deficient of RIM-BP2. These results suggest that the RIM-BP2 function differs between phasic (high release probability, depressing) synapses and tonic (low release probability, facilitating) synapses.

This study reveals that the unique features of hippocampal mossy fiber terminals are low release probability due to the loose coupling between Ca^{2+} channels and vesicles and a large RRP. Furthermore, the study shows that RIM-BP2 controls Ca^{2+} channel density at mossy fiber terminals unlike other mammalian synapses, which may suggest unique molecular compositions of AZ scaffolds.

Acknowledgements

I would like to thank my supervisor, Takeshi Sakaba for continuous guidance, scientific advice, and encouragement during last 7.5 years.

I thank Stephan Sigrist, Dietmar Schmitz and Christian Rosenmund for kindly providing us RIM-BP2 KO mice. I also thank Kenzo Hirose and Stephan Sigrist for insightful comments on my study and The IRCN Imaging Core, The University of Tokyo Institutes for Advanced Studies, for the use of STED microscopy and for assistance. I would like to express my deep gratitude to Takafumi Miki and Hirokazu Sakamoto for technical assistance and scientific advice. This study has not been completed without their support.

I also expand my gratitude to Shigeo Takamori, Hiroaki Misono and Yoshio Sakurai for being my thesis committee members despite of their busy schedule.

I am grateful to the Doshisha University scholarship for doctoral students and the JSPS predoctoral fellowship for financial support.

I am also profoundly grateful to the past and present members in the Sakaba lab and my friends for their encouragement and good time. A special thanks to my family for everything.

Table of contents

1. General introduction

Synapses are an important element for communication between neurons. It is well established that neurotransmitter release from synaptic vesicles is triggered by an elevation of intracellular Ca^{2+} concentration, usually mediated by Ca^{2+} influx via Ca^{2+} channels (Katz, 1969; Südhof, 2012). However, it is not yet clear whether Ca^{2+} acts on other processes of synaptic vesicle cycling, such as synaptic vesicle recruitment (tethering and docking) to the release sites, synaptic vesicle priming at the release sites, and endocytosis. It is also unclear whether there is a common mechanism across synapse types (Zucker & Regehr, 2002; Jackman & Regehr, 2017). Synaptic properties are diverse among central synapses, which are mediated in part by presynaptic mechanisms. Such diversity is essential for a particular type of synapses to be adapted for a specific function in the neural circuits (Dittman et al. 2000). Although technically difficult, direct recordings of presynaptic terminals allow the dissection of the neurotransmitter release mechanisms using capacitance measurements, which have fast time resolution (Neher & Marty, 1982). So far, the measurements are largely limited to large central synapses, such as the calyx of Held (Sun & Wu, 2001; Taschenberger et al. 2002; Wölfel & Schneggenburger, 2003; Schneggenburger & Forsythe, 2006) and ribbon-type synapses (Parsons et al. 1994; von Gersdorff & Matthews, 1994; Neves & Lagnado, 1999; Moser & Beutner, 2000), and measurements in cortical terminals are relatively scarce (Hallermann et al., 2003; Vyleta & Jonas, 2014).

This study focuses on hippocampal mossy fiber terminals and investigates the electrophysiological properties of this synapse. I compare the properties with those of other synapses in the central nervous system (CNS) and discuss similarities and differences. I will first provide an explanation of some terms used in this study.

1.1. Synaptic transmission

Neurons communicate with each other at intercellular junctions called synapses. There are two types of synapses: electrical synapses and chemical synapses. At electrical synapses, pre- and post-synaptic cells are physically connected by pairs of hemichannels, called gap junctions. Gap junctions allow direct transfer of ions and fast communication between neurons. In contrast, chemical synapses communicate using chemical messengers called neurotransmitters. At chemical synapses, an action potential arriving at the presynaptic terminal triggers the opening of voltage-gated Ca^{2+} channels. Ca^{2+} influx through voltage-gated Ca^{2+} channels increases local Ca^{2+} concentration at the release sites. Then, Ca^{2+} triggers synaptic vesicle fusion with the presynaptic membrane and neurotransmitter release from synaptic vesicles within millisecond. Released neurotransmitters diffuse into the synaptic cleft and bind to receptors on the postsynaptic membrane. The Na^{+} and Ca^{2+} influx or Cl^{-} influx into the postsynaptic cells causes excitation or inhibition of the postsynaptic cells, respectively. The entire process of neural communication is called synaptic transmission (Fig. 1).

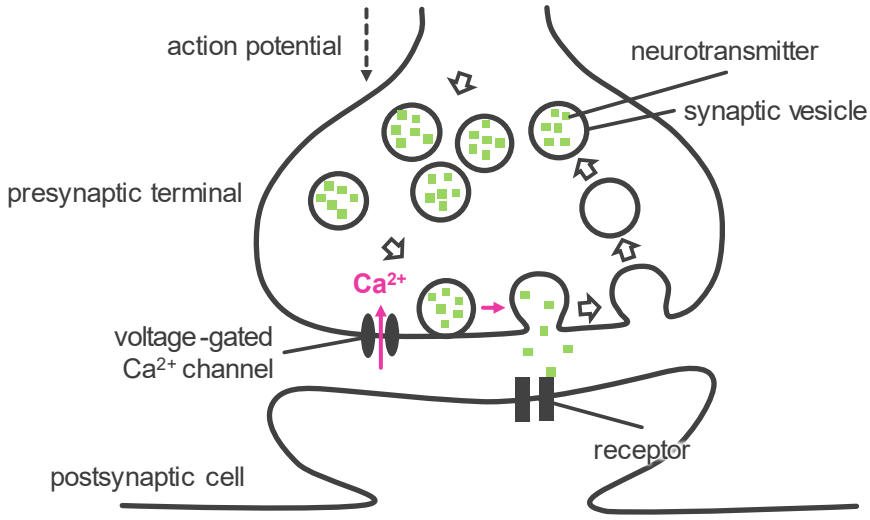

Figure 1. Synaptic transmission at chemical synapses

Upon arrival of an action potential, Ca^{2+} influx through voltage-gated Ca^{2+} channels triggers synaptic vesicle fusion. Synaptic vesicles are recycled within the terminal through endocytosis, refilled with neurotransmitters and replenished to the release site. Released transmitters act on the receptors at the postsynaptic cell, eliciting postsynaptic responses.

1.2. Synaptic vesicle cycle

To maintain synaptic transmission, synaptic vesicles need to be recycled and replenished. When an action potential arrives at the presynaptic terminal, synaptic vesicles fuse with the presynaptic membrane and release neurotransmitters (exocytosis). A group of synaptic vesicles available for immediate exocytosis upon Ca^{2+} influx is defined as a readily releasable pool (RRP). After exocytosis, synaptic vesicle components are retrieved from presynaptic membrane (endocytosis). Retrieved membrane is then used to reform synaptic vesicles, which are eventually refilled with neurotransmitters. The pool of synaptic vesicles which are formed through endocytosis and are fed into the RRP in a few seconds is defined as a recycling pool. Some synaptic vesicles are pre-formed in the terminal and are immobile (resting pool) or are fed into the RRP (reserve pool (RP),

Rizzoli & Betz, 2005; Alabi & Tsien, 2012). In this thesis, I used the term 'RP' instead of 'recycling pool', because electrophysiology could not measure the recycling pool formed from newly-endocytosed vesicles. Synaptic vesicles of the resting pool are recruited to the RP not under basal condition but under strong stimulation. Synaptic vesicles of the RP are recruited to the RRP when the RRP is depleted during and after repetitive stimulation. Thus, synaptic vesicle cycle is needed for sustained synaptic transmission (Rizzoli & Betz, 2005; Denker & Rizzoli, 2010) (Fig. 2A).

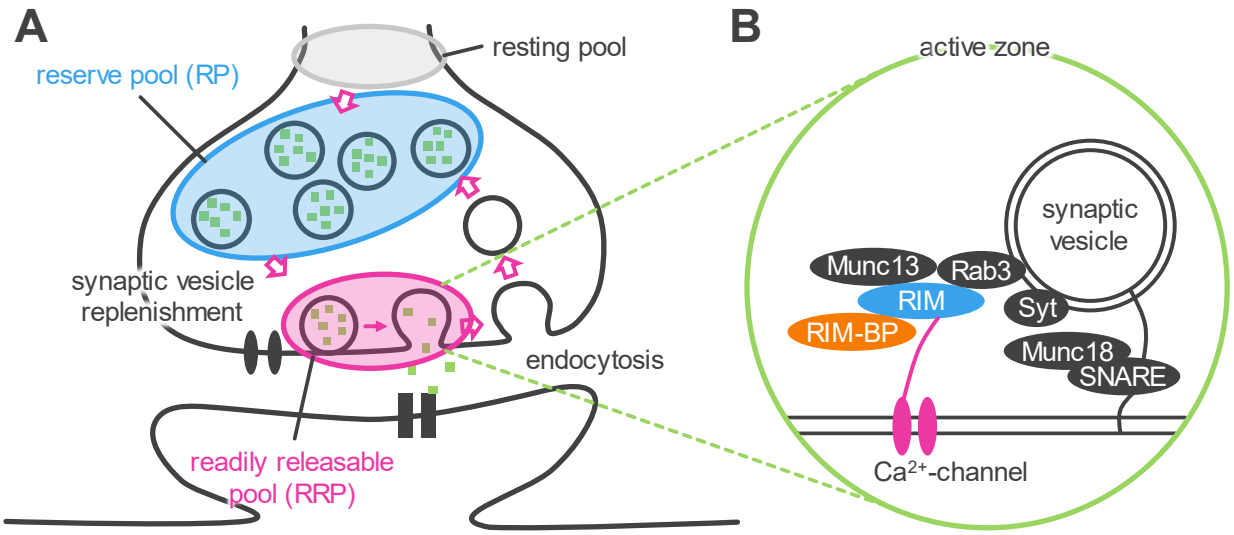

Figure 2. Synaptic vesicle cycle at presynaptic terminals

(**A**) At the presynaptic terminal, synaptic vesicles in the readily releasable pool (RRP) can undergo rapid exocytosis upon Ca^{2+} influx. Released vesicles are retrieved by endocytosis and are deposited to the reserve pool (RP). The RP and RRP could be refilled from the resting pool and the RP, respectively. (**B**) Schematic drawing of the active zone, where various active zone proteins such as Munc13, RIM, and RIM-BP are accumulated to tether synaptic vesicles close to Ca^{2+} channels and prime vesicles for rapid fusion in response to Ca^{2+} influx.

1.3. Active zone

Neurotransmitter release occurs at a specialized region of the presynaptic membrane called the active zone (AZ), where Ca^{2+} channel clusters and release sites are accommodated via AZ-scaffold

proteins (Südhof, 2012) (Fig. 2B). For rapid transmission, accumulation of Ca^{2+} channels, co-localization of Ca^{2+} channels and release sites, and docking and priming of synaptic vesicles are required (Neher and Sakaba, 2008; Neher and Brose, 2018). The differences of these factors may cause synaptic diversity seen among different types of synapses. However, it remains unknown how these factors are regulated by combinations of AZ-scaffold proteins. Revealing the precise functions of AZ-scaffold proteins using KO animals is often difficult because conventional methods such as postsynaptic recordings and imaging cannot measure the underlying mechanisms directly. Rab3-interacting molecule 1 (RIM1) is known to be important for regulating vesicle priming by recruiting Munc13-1 and Ca^{2+} channels (Kiyonaka et al., 2007; Han et al., 2011; Kaeser et al., 2011). Munc13-1 and Munc18 are involved in synaptic vesicle priming, which is supposed to enhance docking of synaptic vesicles to the acceptor complex (SNAREs) at the release sites and convert docked vesicles into the release-ready state (priming). KO of Munc13-1 abolishes evoked release (Augustin et al., 1999) and reduces the number of docked vesicles (Imig et al., 2014). For fusion, SNAREs and synaptogamin1/2 (Syt1/2) are mainly involved in rapid fusion upon Ca^{2+} influx (Haucke et al., 2011), though the precise mechanisms are still unknown. Moreover, other proteins such as RIM-BP2, bassoon and piccolo are known for AZ-scaffold proteins, but the functional roles are less clear.

1.4. Ca^{2+}-dependence of synaptic vesicle cycle

It is well known that Ca^{2+} triggers exocytosis of synaptic vesicles and that synaptotagmin1/2

is a putative Ca^{2+} sensor for exocytosis (Katz, 1969; Sun et al., 2007). In addition to exocytosis, other steps of synaptic vesicle cycling are supposed to be Ca^{2+}-dependent. Vesicle replenishment to the RRP is considered to be Ca^{2+}-dependent at some synapses (Zucker & Regehr, 2002; Miki et al., 2018). At the calyx of Held, it is well established that vesicle replenishment is Ca^{2+}-dependent and requires C2 domains and calmodulin binding domain of Munc13-1 (Lipstein et al., 2013, 2021), a priming protein. In addition to Munc13-1, Ca^{2+} sensitive proteins, such as synaptotagmin3 (Weingarten et al., 2022) might be relevant. However, it is unclear if replenishment is Ca^{2+}-dependent in other synapses. It is also unclear about the detailed molecular mechanisms of vesicle replenishment. Endocytosis is Ca^{2+}-dependent at the calyx of Held (Hosoi et al., 2009; Wu et al., 2009). However, it is unclear if this applies to other synapses including mossy fiber terminals, and Ca^{2+} sensor for endocytosis remains unclear. Molecular mechanisms of endocytosis remain to be identified though candidate proteins such as clathrin, dynamin, and intersectin have been listed (Saheki & De Camilli, 2012). Identification of Ca^{2+}-sensitive steps in vesicle cycle is fundamental for understanding the mechanisms of short- and long-term plasticity, because dynamics of vesicle pools affect synaptic strength profoundly (Zucker and Regehr, 2002).

1.5. Ca^{2+} channel-release site coupling

The efficacy of synaptic transmission is not constant, and activity-dependent changes in the synaptic strength is called synaptic plasticity. The facilitation and depression of synaptic strength lasts

for several minutes (short-term synaptic plasticity) or for several hours (long-term synaptic plasticity). Short-term synaptic plasticity plays a crucial role in information processing (Fortune & Rose, 2001; Deng & Klyachko, 2011), and long-term synaptic plasticity is considered cellular basis of learning and memory. The probability of neurotransmitter release, vesicle pool dynamics, desensitization and saturation of postsynaptic receptors, and the number of available receptors all potentially contribute to the extent of synaptic plasticity. In particular, short-term facilitation is mainly caused by the modulation of release probability. At presynaptic terminals, the coupling distance between Ca^{2+} channels and release sites regulates the release probability of synaptic vesicles (Neher & Sakaba, 2008). The coupling between Ca^{2+} channels and release sites is tight at synapses having high release probability vesicles, such as calyx of Held synapses. In contrast, at synapses having low release probability vesicles, the coupling is loose (Eggermann et al., 2011; Vyleta & Jonas, 2014). One type of AZ proteins interacts with other types of AZ proteins, Ca^{2+} channels, and synaptic vesicles, and such AZ complexes contribute to Ca^{2+}-channel tethering to the AZ and synaptic-vesicle docking/priming (Mukherjee et al., 2010; Kaeser et al., 2011; Han et al., 2011; Davydova et al., 2014). As such, AZ protein complexes control the coupling distances between Ca^{2+} channels and synaptic vesicles and modulate synaptic efficacy. To reveal the function of AZ proteins at synapses may lead to an understanding of the synaptic plasticity.

1.6. Hippocampal mossy fiber-CA3 synapse

Hippocampal mossy fibers form a large presynaptic terminal onto CA3 pyramidal cells and have an important function in hippocampal circuits (Lawrence & McBain, 2003; Mori et al., 2004; Nicoll & Schmitz, 2005; Vyleta et al., 2016). Mossy fibers have several unique features. Transmitter release probability is low, and the mossy fiber synapses exhibit pronounced facilitation during repetitive stimulation. In addition, robust long-term potentiation is observed, which is mediated by a presynaptic, cAMP-dependent mechanism (Nicoll & Schmitz, 2005). The terminal comprises one of the few cortical terminals, which has a diameter of ~5 μm and is sufficiently large to be accessible by patch pipettes (Geiger & Jonas, 2000) (Fig. 3).

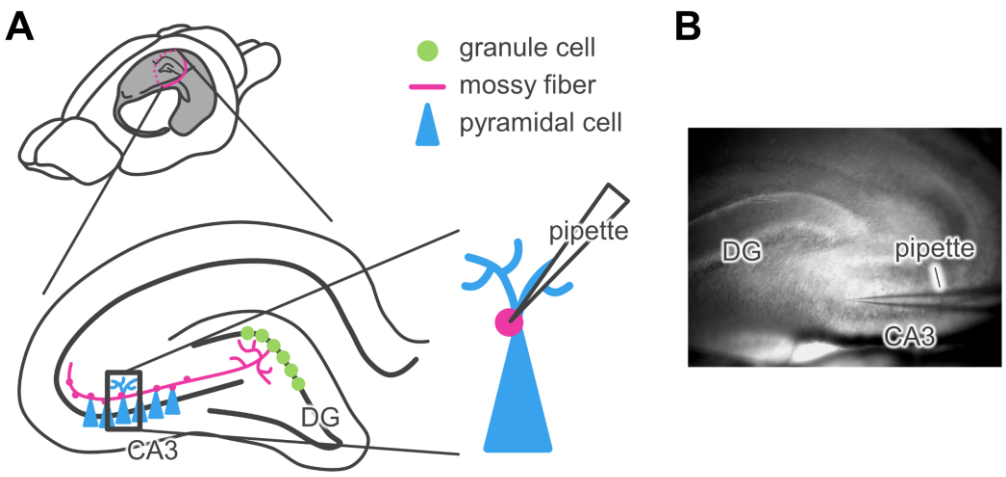

Figure 3. Schematic drawing and micrograph of hippocampal slice

Schematic drawing (**A**) and micrograph (**B**) of hippocampal slice. Mossy fibers are axons of granule cells in dentate gyrus (DG). Mossy fibers extend toward CA3 region and synapse onto CA3 pyramidal cells. Mossy fiber terminals are accessible by patch pipettes.

2. Ca^{2+}-dependence of synaptic vesicle exocytosis and endocytosis at the hippocampal mossy fiber terminal.

2.1. Introduction

Previously, presynaptic capacitance measurements have been applied to the mossy fiber terminal to measure the kinetics of exo- and endocytosis (Hallermann et al., 2003; Delvendahl et al., 2016; Midorikawa & Sakaba, 2017). However, Ca^{2+}-dependence of exocytosis and endocytosis has not been examined thoroughly using exogenous Ca^{2+} buffers. Although the buffer sensitivity of action potential-evoked release has been examined (Vyleta & Jonas, 2014), the effect of buffers on the depletion time course of the RRP of synaptic vesicles has not been investigated. More importantly, it remains unknown whether synaptic vesicle replenishment to the RRP and endocytosis have any Ca^{2+}-dependence. In the present study, I analyzed the kinetics of exocytosis, endocytosis and synaptic vesicle replenishment and their sensitivity to Ca^{2+} buffers quantitatively. I found that exocytosis was sensitive to Ca^{2+} buffers, whereas synaptic vesicle replenishment to the RRP and endocytosis were relatively insensitive.

2.2. Material and Methods

2.2.1. Ethical approval

All animal procedures were conducted in accordance with the guidelines of the Physiological

Society of Japan and were approved by Doshisha University committee for Regulation on the Conduct of Animal Experiments and Related Activities. All efforts were taken to minimize animal numbers.

2.2.2. Animal care

Rats were given food and water freely and housed under 12:12 h light/dark cycles in a temperature controlled animal facility.

2.2.3. Slice preparation

Male and female Wistar rats (postnatal days 19-28) were deeply anaesthetized with evaporated isoflurane (1-3%), rapidly sacrificed by decapitation and then their brains were removed. Transverse hippocampus slices (300 μm thick) were obtained using a Leica VT1200S slicer (Leica Microsystems, Wetzlar, Germany) in ice-cold slice medium contained (in mM) 87 NaCl, 75 sucrose, 25 $NaHCO_3$, 1.25 NaH_2PO_4, 2.5 KCl, 10 glucose, 0.5 $CaCl_2$ and 7 $MgCl_2$ (Hallermann et al., 2003). Slices were incubated at 37°C for >0.5 h in a slice medium gassed with 95% O_2 and 5% CO_2, and were left at room temperature afterwards up to 4 h (22-25°C). For slice electrophysiological recordings, slices were visualized on an upright microscope (BX-51; Olympus, Tokyo, Japan) in slice recording solution contained (in mM) 125 NaCl, 2.5 KCl, 25 glucose, 25 $NaHCO_3$, 1.25 NaH_2PO_4, 0.4 ascorbic acid, 3 myoinositol, 2 Na-pyruvate, 2 $CaCl_2$ and 1 $MgCl_2$ (pH 7.4, gassed with 95% O_2

and 5% CO_2).

2.2.4. Whole-cell recordings

For electrophysiological recordings, 1 μM tetrodotoxin (TTX) was added to block Na^+ channels. Recordings were performed at room temperature (22-25°C) within 4 h after cutting the slices. Hippocampal mossy fiber terminals were whole-cell voltage clamped at -80 mV using EPC10/3 amplifier (HEKA, Bolanden, Germany), controlled by Patchmaster software (HEKA). The patch pipettes were filled with intracellular solution containing (in mM): 135 Cs-gluconate, 20 TEA-Cl, 10 HEPES, 5 Na_2-phosphocreatine, 4 MgATP, 0.3 GTP and 0.5 ethylene glycol tetraacetic acid (EGTA) (pH 7.2). In some experiments, the concentration of EGTA was changed to 0.1 mM, 1 mM and 5 mM, or was replaced with 1 mM 1,2-bis(2-Aminophenoxy)ethane-N,N,N',N'-tetraacetic acid (BAPTA). Liquid junction potential was not corrected. Membrane currents were low-pass filtered at 2.9 kHz and sampled at 20 kHz. Membrane capacitance measurements were performed using an EPC10/3 amplifier in the sine + DC configuration (Gillis, 2000) using Patchmaster software (HEKA, Germany). A sine wave (30 mV in amplitude, 1000 Hz in frequency) was superimposed on a holding potential of -80 mV. Presynaptic patch pipettes (GC150F-10; Harvard Apparatus, Cambridge, MA, USA) had a resistance of typically 15-20 MΩ (slice). Average series resistance was 65 ± 1.6 MΩ (n = 84). R_s compensation was not used in the present study. I stopped recordings when the leak currents exceeded 100 pA at resting potential. Series resistance changes possibly affected capacitance traces,

especially when measuring the time course of endocytosis. I stopped the recordings when such artefacts became serious. The whole-cell recordings usually lasted 10-15 min without significant exocytosis rundown. Whole-cell dialysis could potentially cause washout of soluble proteins including endogenous Ca^{2+} buffers (Vyleta & Jonas, 2014).

2.2.5. Analysis

The data were analyzed by Igor Pro (WaveMetrics, Lake Oswego, OR, USA) or Excel (Microsoft Corp, Redmond, WA, USA). In some cases, a line or an exponential fit was performed using Igor Pro. To fit the pulse train data, I simulated the vesicle pool models with numerical integration using Igor Pro. In the serial model, the vesicles are recruited from the resting pool to the RP and then to the RRP. In the serial model, the number of vesicles in the two pools (N_{RRP} and N_{RP}) are defined by the differential equations:

$$\frac{d}{dt}N_{RRP}(t) = -k_{rel}N_{RRP}(t) + k_{rec,RRP}\big(N_{RP}(t) - N_{RRP}(t)\big) \qquad (1)$$

$$\frac{d}{dt}N_{RP}(t) = -k_{rec,RRP}N_{RP}(t) + k_{rec,RP}\big(N_{RP}(0) - N_{RP}(t)\big) \qquad (2)$$

where k_{rel} is a release rate constant of the RRP, $k_{rec,RRP}$ is a recruitment rate constant from the RP to the RRP and $k_{rec,RP}$ is a refilling rate constant for the RP. When t = 0, the RRP and the RP are fully occupied by vesicles and the size of the pools are equal ($N_{RRP}(0) = N_{RP}(0)$). To limit the size of the two pools and keep the equilibrium between the pools before pulse stimulations, I defined the rate of the recruitment from the RRP to the RP as a value equal to $k_{rec,RRP}$. In the RP, empty sites are refilled

with the rate constant $k_{rec,RP}$. Only during depolarization pulses, vesicle release is assumed to occur (thus, $k_{rel} = 0$ during intervals between pulses, and before and after pulses). In the case of 5 mM EGTA, k_{rel} constantly increases with pulse number (k_{rel} = 7 s^{-1} for the first pulse) and reaches 33 s^{-1} at the fourth pulse. Then, k_{rel} keeps the maximum value (33 s^{-1}) until the last pulse.

The second model (modified serial model) is essentially the same as the serial model, although synaptic vesicles fuse with the plasma membrane from both the RRP and the RP. In the third model (parallel model), vesicles in the resting pool are recruited to the RRP and the RP in parallel, and vesicles fuse with the plasma membrane from both the RRP and the RP (Fig. 4).

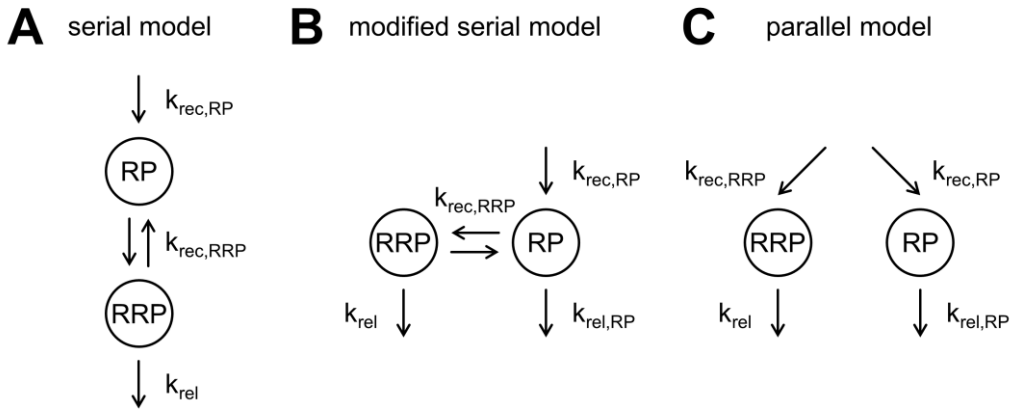

Figure 4. Vesicle pool model

(**A**) Serial model: synaptic vesicles are released from the RRP with a rate constant k_{rel}. The RP is refilled with a rate constant $k_{rec,RP}$, and $k_{rec,RRP}$ is a recruitment rate constant from the RP to the RRP. (**B**) Modified serial model: synaptic vesicles are released from the RRP and the RP with a rate constant k_{rel} and $k_{rel,RP}$, respectively. The RP is refilled with a rate constant $k_{rec,RP}$, and $k_{rec,RRP}$ is a recruitment rate constant from the RP to the RRP. (**C**) Parallel model: synaptic vesicles are released from the RRP and the RP with a rate constant k_{rel} and $k_{rel,RP}$, respectively. The RRP and RP are refilled with a rate constant $k_{rec,RRP}$ and $k_{rec,RP}$, respectively.

2.2.6. Statistical analysis

In some cases, t test and ANOVA were used for statistical analysis.

2.3. Results

2.3.1. Kinetics of exocytosis at the hippocampal mossy fiber terminal.

During exocytosis, synaptic vesicles fuse with presynaptic membrane and increase membrane surface area. Capacitance measurements can measure the number of released vesicles as changes in membrane capacitance. A depolarizing pulse induces exocytosis, and stimulus trains or a long depolarizing pulse can deplete the readily releasable pool (RRP) of synaptic vesicles. By using capacitance measurements, I can measure the size and the release kinetics of the readily releasable pool (RRP) of synaptic vesicles at room temperature. I applied whole-cell patch-clamp recordings and capacitance measurements to hippocampal mossy fiber terminals in acute slices from Wistar rats (postnatal day 19-28). The patch pipette contained Cs^+-based internal solution and 0.5 mM EGTA. The external solution contained 1 μM TTX to block Na^+ currents. The terminal has the basal capacitance of 1-4 pF, consistent with Hallermann et al. (2003). When the terminal was depolarized from -80 mV to 0 mV, Ca^{2+} currents were activated with a time constant of 1.6-12 ms (7.2 ± 2.0 ms, n = 21) and stayed constant afterwards (Fig. 5A and B). Capacitance jumps were elicited in response to presynaptic Ca^{2+} influx. In the example of Figure 5A, capacitance jumps became larger as the duration of the depolarizing pulse was prolonged, but the increase was saturated at a 100 ms pulse. The amplitude of capacitance jump in response to a 100 ms pulse was 50-60 fF (53 ± 3.7 fF, n = 25), corresponding to fusion of 500-600 vesicles. This estimate was made based on an assumption that a single vesicle fusion causes a capacitance jump of ~100 aF, according to the previous study comparing

capacitance jumps and cumulative release estimated from the EPSC deconvolution method (Midorikawa & Sakaba, 2017). However, the number of released vesicles could be underestimated, because previous EM studies indicate the vesicle diameter of 30-50 nm (Henze et al., 2002; Rollenhagen et al., 2007), and this would predict the capacitance jump of 30-70 aF per vesicle (based on the assumption of specific membrane capacitance of 1 μF cm^{-2}, see also Hallermann et al., 2003; He et al., 2006). Then, the number of vesicles would be much larger than 500 vesicles (700-1600 vesicles). Figure 5B plots the relationship between the pulse duration and the capacitance jumps. The time course of capacitance increase could be fitted by a single exponential of 41 ms, with a maximal value of 57 fF. Activation of Ca^{2+} currents was relatively slow compared with previous measurements (0.79 ± 0.05 ms: Li et al., 2007; Fig. 5B, bottom), and the time course of release was somewhat slowed due to the activation time course of Ca^{2+} currents. Slow Ca^{2+} current activation could be due to the differences in experimental conditions used, e.g. R_s and temperature. Ca^{2+} current amplitudes were variable among terminals, but were only shallowly correlated to the capacitance jumps in response to a 100 ms pulse (Fig. 5C), suggesting that the RRP sizes are independent of Ca^{2+} current amplitudes. This result is consistent with Hallermann et al. (2003). Also, capacitance jumps were shallowly correlated with the baseline C_m (Fig. 5D), suggesting that the RRP was larger with the terminal size.

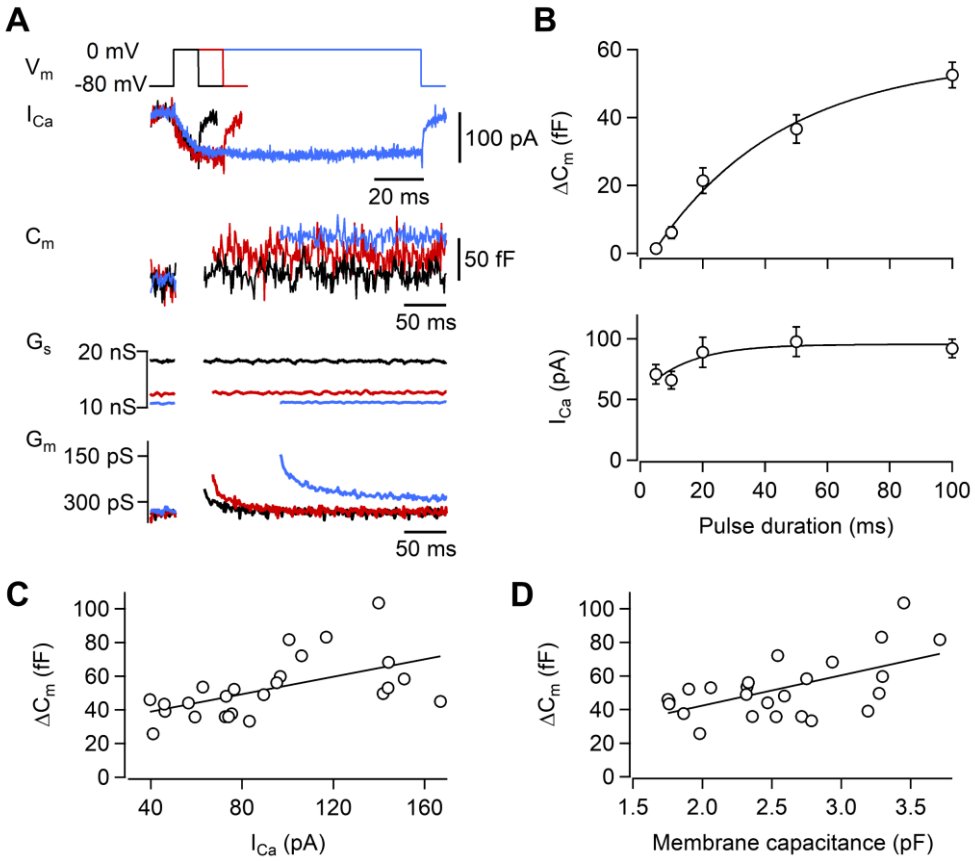

Figure 5. Capacitance measurements at the hippocampal mossy fiber terminal

(**A**) The terminal was depolarized from -80 mV to 0 mV for 10, 20 and 100 ms *(top)*. Ca^{2+} currents *(middle)*, membrane capacitance (C_m), series conductance (G_s), membrane conductance (G_m) are shown. (**B**) Top panel shows the amplitudes of capacitance increase plotted against the pulse duration. An exponential fit is superimposed. Bottom panel shows the peak Ca^{2+} current amplitudes plotted against the pulse duration. (**C**) The capacitance jumps in response to a 100 ms pulse were plotted against Ca^{2+} current amplitudes. Each data point represents the data from each terminal. The patch pipette contained 0.5 mM EGTA. A line fit was $\Delta C_m = 28.6 + 0.26\ I_{Ca}$ (fF), and correlation coefficient was 0.55. (**D**) The capacitance jumps in response to a 100 ms pulse were plotted against the basal membrane capacitance. A line fit was $\Delta C_m = 6.3$ fF $+ 18.0\ C_m$ (fF), and correlation coefficient was 0.58.

Previous studies have used Ca^{2+} buffers to examine the coupling between Ca^{2+} channels and transmitter release (Adler et al., 1991; Borst et al., 1995; Borst & Sakmann, 1996). Vyleta and Jonas (2014) have examined the effects of Ca^{2+} buffers on action potential-evoked transmitter release at hippocampal mossy fiber-CA3 synapses, but the dependence on the time course of vesicle pool

depletion has not been examined. In order to examine the dependence of vesicular release on Ca^{2+} buffers, I have first changed the concentration of EGTA in the patch pipette (Fig. 6A). In the presence of 0.1 mM EGTA (low Ca^{2+} buffer condition), the capacitance jump in response to a 100 ms pulse (65 ± 7.1 fF, n = 19) was larger than that under 0.5 mM EGTA. Figure 6B shows the capacitance jump plotted against the pulse duration. The capacitance jumps were larger than those under 0.5 mM EGTA. In the presence of 0.1 mM EGTA, the time course could be fitted by a single exponential with a time constant of 30 ms, and the maximal value was 68 fF. Based on the data from 0.1 mM EGTA, I estimate that the RRP size expressed in membrane capacitance changes was 60-70 fF (600-700 vesicles) at mossy fiber terminals. This also suggested that the RRP was largely depleted by a 100 ms pulse under 0.5 mM EGTA.

In contrast, 5 mM EGTA suppressed the capacitance jumps in response to a 100 ms pulse considerably (Fig. 6A, 29 ± 4.1 fF, n = 12). When the time course of release was plotted (Fig. 6B), a linear relationship between the capacitance jumps and the pulse duration was observed. Ca^{2+} currents were larger under 5 mM EGTA, which may suggest that Ca^{2+} currents may be slightly inactivated by Ca^{2+}. However, the differences from control conditions were not statistically significant (ANOVA test). In addition, the peak Ca^{2+} current amplitudes were variable among terminals (40-150 pA) and had only a weak correlation to the capacitance jumps in the previous study (Fig. 5C, Hallermann et al., 2003). BAPTA has the same Kd as EGTA, but has a faster biding rate compared to EGTA (Adler et al., 1991). 1 mM BAPTA suppressed the release at shorter pulses (10 and 20 ms), but no difference

from the 0.5 mM EGTA condition was found at 100 ms ($p = 0.6$). This most likely suggests that BAPTA was locally saturated around the release sites at longer pulses. Theoretical studies have suggested that local saturation happens around the release sites, relieving buffer-mediated inhibition of local Ca^{2+} at the release sites and causing facilitation of transmitter release (Rozov et al., 2001; Vyleta & Jonas, 2014). Buffer saturation happens only if (1) the coupling between Ca^{2+} channels and the synaptic vesicle is loose (loose coupling, Borst & Sakmann, 1996; Neher, 1998) and (2) the buffer has a fast Ca^{2+} binding rate like BAPTA (not EGTA). Consistently, when the capacitance jump was plotted against the amounts of Ca^{2+} influx (pooling all the data from different terminals in response to a 50 ms or 100 ms pulse), there is a non-linear relationship between the amounts of Ca^{2+} influx (Ca^{2+} charge) and capacitance jumps (Fig. 6C). Saturation of BAPTA is consistent with Vyleta and Jonas (2014), examining the effect of BAPTA on paired-pulse facilitation. I should note that Vyleta and Jonas (2014) have examined action potential-induced release and used lower concentration whereas I have used long depolarization and used higher concentration (1 mM).

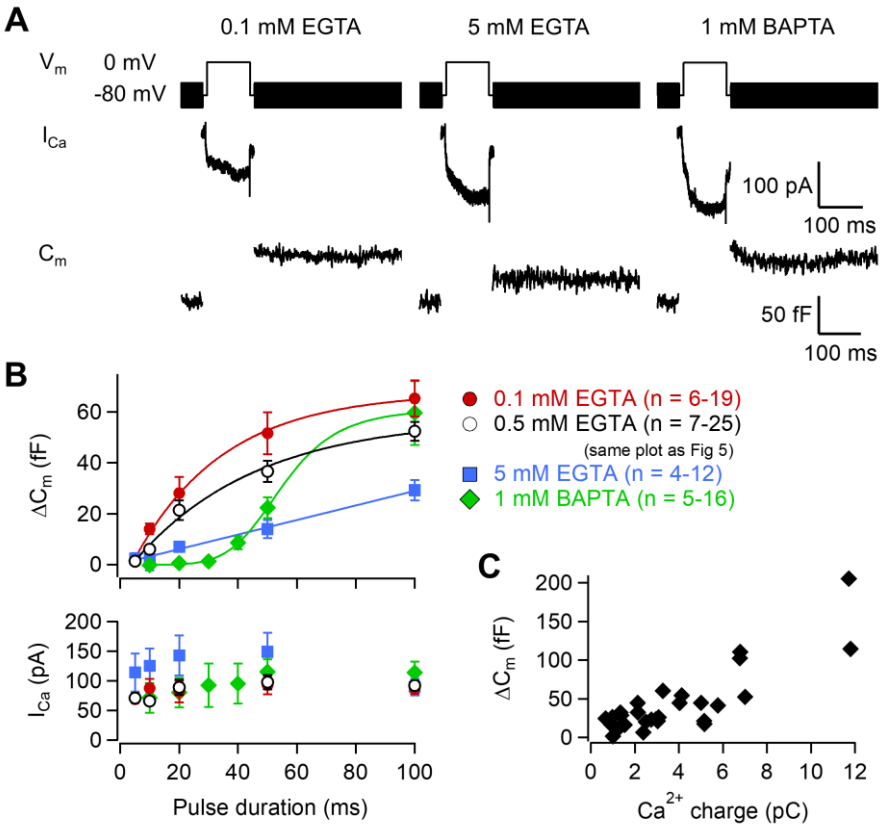

Figure 6. The effects of Ca buffers on synaptic vesicle exocytosis

(**A**) The terminal was depolarized from -80 mV to 0 mV for 100 ms. From left, 0.1 mM EGTA, 5 mM EGTA, and 1 mM BAPTA were introduced to the terminal. Membrane potential (V_m), Ca^{2+} currents (I_{Ca}), and membrane capacitance (C_m) are shown. (**B**) Top panel shows the relationship between capacitance jumps and pulse duration in various conditions. Bottom panels show the relationship between the peak Ca^{2+} current amplitudes and pulse duration. Filled circles, open circles, filled square and filled diamonds represent the data from 0.1 mM EGTA, 0.5 mM EGTA, 5 mM EGTA and 1 mM BAPTA, respectively. Fits are superimposed on the data. The fit for 1 mM BAPTA is a Hill equation, and others are an exponential. (**C**) The capacitance jumps are plotted against the amounts of Ca^{2+} influx calculated from Ca^{2+} currents in 1 mM BAPTA. The pulse duration was 50 or 100 ms and the data were pooled across terminals. As the amount of Ca^{2+} influx increases, the capacitance jump increases supralinearly, suggesting that BAPTA is locally saturated. Ca^{2+} influx was calculated from the amounts of Ca^{2+} influx measured from Ca^{2+} currents and was converted to Ca^{2+} charge by using integration of Ca^{2+} currents during the pulse.

2.3.2. Kinetics of synaptic vesicle replenishment measured by the dual pulse protocol at the hippocampal mossy fiber terminal.

To examine the rate of vesicle replenishment to the RRP, I applied a dual pulse protocol to

the mossy fiber terminal. The patch pipette contained 0.5 mM EGTA. A pair of a 100 ms pulse (to 0 mV) was applied with an interval of 500 ms and 5 s in the example of Figure 7A. In Figures 5 and 6, I show that a 100 ms pulse was sufficient to deplete the RRP to a large extent, so that the second pulse should monitor the recovery from depletion. With an interval of 500 ms, the capacitance jump recovered to 46% (43 ± 4.3% on average) in this example. With an interval of 5 s, it recovered to 76% (79 ± 5% on average) of the initial value. In Figure 7B, the recovered fraction of the capacitance jump is plotted against the stimulus interval. The time course of recovery could be fitted by a single exponential with a time constant of 0.89 s. At a 10 s interval, the capacitance jumps were recovered to 77%. The RRP was not fully recovered at this interval, although the capacitance recovered fully when waiting for a sufficient time (Fig. 7B). It is probable that the slow component of recovery exists (Midorikawa & Sakaba, 2017). Ca^{2+} currents were reduced at the shortest interval but were recovered much faster than the recovery of capacitance responses, indicating that the recovery of capacitance responses largely reflected that of the vesicle pool.

When the concentration of EGTA was increased to 5 mM, a 100 ms pulse could not deplete the RRP and the second pulse elicited a similar capacitance jump as the first one (data not shown). Therefore, I could not examine the recovery rate under 5 mM EGTA and I reduced the concentration of EGTA to 1 mM (see below the repetitive stimulation experiment to estimate the replenishment rate under 5 mM EGTA). Although 1 mM EGTA is below the reported IC50 value for EGTA for transmitter release at the mossy fiber synapse (Vyleta & Jonas, 2014), transmitter release is triggered

by local Ca^{2+} close to Ca^{2+} channels and synaptic vesicle replenishment is often driven by residual Ca^{2+} (Dittman & Regehr, 1998; Stevens & Wesseling, 1998; Wang & Kaczmarek, 1998). I expected that the increase in the buffer concentration to 1 mM should buffer residual Ca^{2+} sufficiently and slow vesicle replenishment sufficiently if the recovery is driven by residual Ca^{2+}. Under the condition of 1 mM EGTA, a 100 ms pulse elicited capacitance jumps of ~50 fF (47 ± 7.2 fF, n = 6), suggesting that the RRP was still depleted to a large extent and the double pulse protocol could be used for monitoring recovery from the RRP depletion. When the recovered fraction was plotted against the stimulus interval (Fig. 7B), the recovery time course could be almost indistinguishable from that in the presence of 0.5 mM EGTA in the patch pipette and the time course could be fitted by a single exponential with a time constant of 1.30 s. Conversely, when the EGTA concentration was reduced to 0.1 mM, the capacitance increase in response to the second pulse was somewhat smaller for very short intervals compared to the 0.5 mM EGTA condition (Fig. 7B) (for possible explanations, see the Discussion). Nevertheless, when the recovered fraction was plotted against the stimulus interval, the overall time course was similar to that under 0.5 mM EGTA. The time course could be fitted by a single exponential with a time constant of 0.85 s. Taken together, recovery from the RRP depletion appears to be insensitive to Ca^{2+} buffers in the range of 0.1-1 mM EGTA.

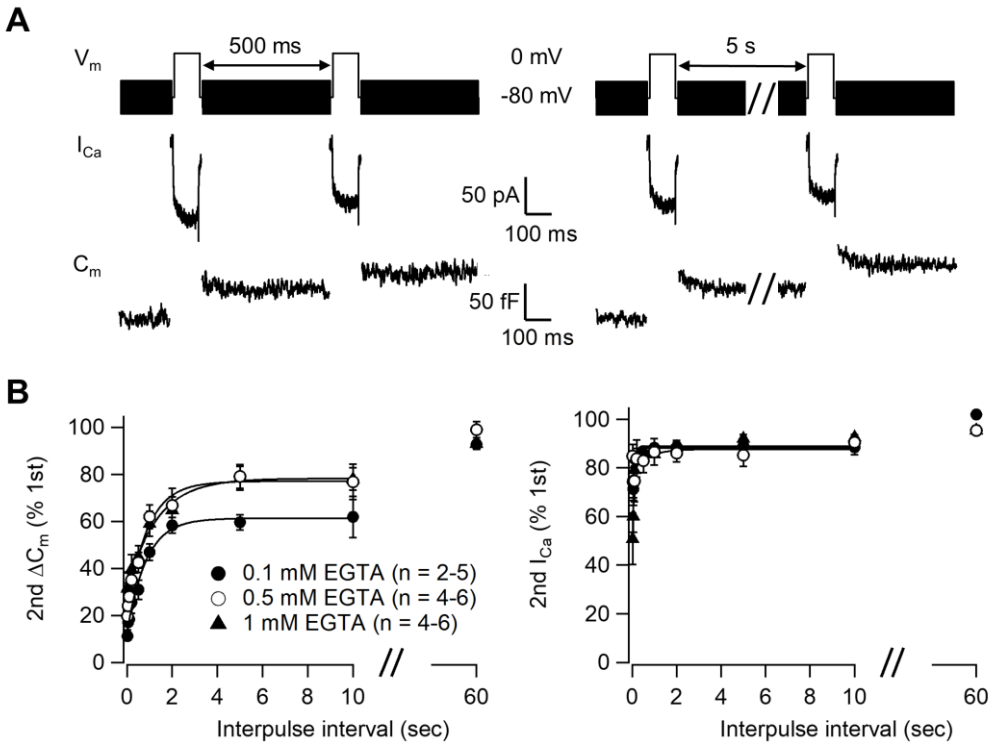

Figure 7. The double-pulse protocol to monitor recovery of the RRP

(**A**) The terminal was depolarized from -80 mV to 0 mV for 100 ms twice with variable intervals (500 ms and 5 s in left and right panel, respectively). From top, membrane potential (V_m), Ca^{2+} currents (I_{Ca}), and membrane capacitance (C_m) are shown. (**B**) The recovered fraction of the second response (C_m) is plotted against the stimulus interval (interpulse interval). The data from 0.1 mM (filled circles), 0.5 mM (open circles) and 1 mM EGTA (filled triangles) are shown. Each data set is fitted by an exponential (the interval up to 10 s). Right panel shows the relationship between the peak Ca^{2+} current amplitudes and pulse duration. At 60 s, the first responses of two successive double pulses were compared.

2.3.3. Measurement of the synaptic vesicle replenishment rate using repetitive stimulation.

Synaptic vesicle replenishment could be monitored by repetitive stimulation of 100 ms pulses. This protocol could deplete the RRP eventually even under a high EGTA condition (such as 5 mM EGTA), where a single 100 ms could not deplete the RRP fully. I applied a 100 ms pulse (to 0 mV) 10 times with an interval of 250 ms in the presence of 0.5 mM EGTA in the patch pipette (Fig. 8A). After the second or the third pulse, capacitance jumps were reduced and stayed constant at

subsequent pulses. Ca^{2+} currents were inactivated during repetitive stimulation (Fig. 8B) and the decrease in capacitance jumps could be a result of the reduced Ca^{2+} influx (although the increase in the residual Ca^{2+} may have counteracted). To elicit more constant Ca^{2+} influx during repetitive pulses, the terminal was depolarized to -10 mV to reduce the amounts of Ca^{2+} influx and possible Ca^{2+}-dependent inactivation of Ca^{2+} currents (Fig. 8A). The capacitance jump in response to the first pulse was somewhat decreased but, again, the cumulative capacitance jumps were converged to those under the 0 mV pulse condition (see below).

Figure 8B plots the cumulative increases of capacitance over the stimulus number. Back-extrapolation of a line fit (to the later part of the cumulative plot) toward the first stimulation gave the y-intercept of 84 fF, which was similar or even somewhat larger than the RRP size. However, this value is a lower estimate for the vesicle pool because back extrapolation assumes constant vesicle replenishment from the first stimulation and/or the vesicle pool was incompletely depleted (Neher, 2015). Therefore, the initial vesicle pool size is probably larger than the RRP value. A vesicle pool model has to be constructed to estimate the size of the vesicle pools. The -10 mV protocol provided somewhat a smaller value of the y-intercept (Fig. 8B), most probably reflecting the vesicle pool not being entirely depleted within the initial few pulses (Neher, 2015). As seen below, the overall kinetics of cumulative release under conditions of 0 mV and -10 mV could be explained by a simple model assuming the same size of vesicle pools. The vesicle replenishment rates (estimated from the slope of a line fit) were similar between 0 mV and -10 mV protocols and had a rate of 9.0-9.2 fF per stimulus

(equal to 36 fF/s). Assuming that the RRP size was ~60 fF (Figs 5 and 6), the rate constant of synaptic vesicle recruitment to the RRP should be ~1-2 s. The time scale is similar to rapid recovery time constant of the RRP (~1 s) estimated from the dual pulse protocol. The data also suggested that synaptic vesicle replenishment was not significantly influenced by the amounts of Ca^{2+} influx.

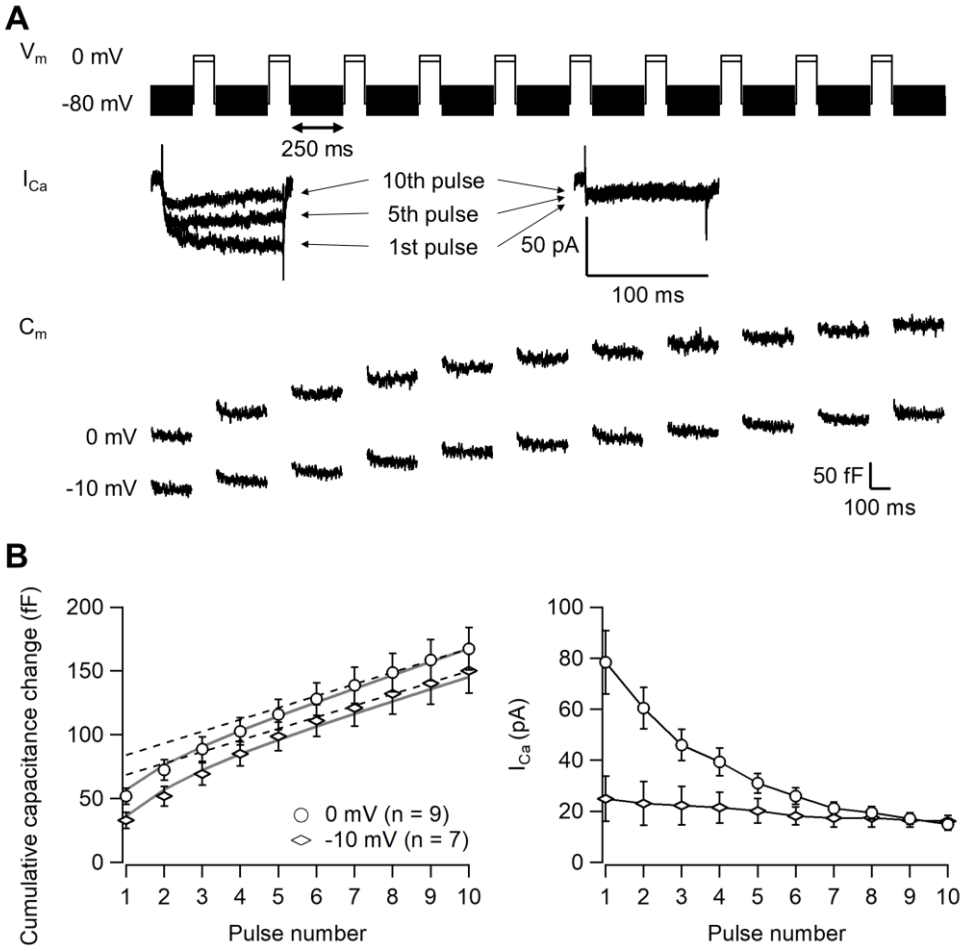

Figure 8. Repetitive stimulation to deplete the vesicle pools and measure the rate of synaptic vesicle replenishment

(A) The terminal was depolarized 10 times, from -80 mV to 0 mV or -10 mV for 100 ms with the stimulus interval of 250 ms. The example traces are shown in the bottom panel. Insets show the Ca^{2+} currents observed in 0 mV and -10 mV conditions *(left and right)*. (B) The cumulative capacitance jumps *(left)* and Ca current amplitudes *(right)* are plotted against the stimulus number. The 0 mV (open circles) and -10 mV (open diamonds) conditions are shown. Dotted lines show the extrapolation of the line fit to the later part of the train (last 3 responses) to the y-intercept. Gray lines show the simulation of the serial pool model.

To examine sensitivity of vesicle replenishment to Ca^{2+} buffers, I changed the concentration of EGTA to 0.1 mM and 5 mM (Fig. 9A) and applied the repetitive stimulation protocol (to 0 mV) to the mossy fiber terminal. Example traces of these two conditions are shown in Figure 9A. Figure 9B plots the cumulative capacitance increases under different concentrations of EGTA (0.1 mM, 0.5 mM and 5 mM EGTA). As shown in Figure 6, the capacitance jumps in response to the first pulse were larger as the EGTA concentration was lower. However, as the stimulation went on, the cumulative values converged to similar values of ~170 fF toward the end of the stimulation protocol. Back extrapolation of a line fit toward the first stimulation indicates a capacitance value of ~100 fF (95 fF for 0.1 mM, 101 fF for 5 mM EGTA), similar to or somewhat larger than the RRP size. The line fit could be used for estimating the vesicle replenishment rate and the rate constants were similar among three conditions (7-9 fF per stimulus; 9.2 fF for 0.1 mM, 7.7 fF for 5 mM EGTA). The data suggested that the rates of synaptic vesicle replenishment were insensitive to Ca^{2+} buffers under our experimental conditions.

To explain the train data quantitatively, I fitted them with the vesicle pool model. The simplest model with a single vesicle pool and constant vesicle replenishment rate could not fit the data, and a two-pool model has to be postulated. In the serial pool model, vesicles in the resting pool are recruited to the reserve pool (RP) and then are recruited from the RP to the RRP. Vesicle fusion takes place only from the RRP. I have simulated the model to explain the train data under conditions of 0 mV and -10 mV (Fig. 8), and under different Ca^{2+} buffering conditions (0.1, 0.5, and 5 mM

EGTA) (Fig. 9), as indicated by the grey lines in Figures 8B and 9B. The serial model explained these conditions by assuming fixed rate constants of vesicle recruitment. Both the RRP and the RP have the size of 60-65 fF. In any case, the recruitment rate constant from the resting pool to the RP was estimated to be 1 s^{-1} and the recruitment rate constant from the RP to the RRP was estimated to be 1.2 s^{-1}, which is similar to the vesicle replenishment rate constant estimated from the double pulse experiment (time constant of 0.85-1.3 s). The only differences among the three conditions were the release rate constants from the RRP (0.1 mM EGTA: 33 s^{-1}; 0.5 mM EGTA: 24 s^{-1}; 5 mM EGTA: 7 s^{-1}). A better fit of the plot for 5 mM EGTA was obtained by increasing the rate constant constantly up to 33 s^{-1} with stimulus number. I do not exclude other two pool models with more free parameters (parallel pool model and modified serial model; see Methods) because they could fit the data more or less equally (data not shown). The important point here is that the data are consistent with the model assuming two pools (the RRP and the RP), as well as Ca^{2+}-independent vesicle recruitment, with a time constant of 1 s.

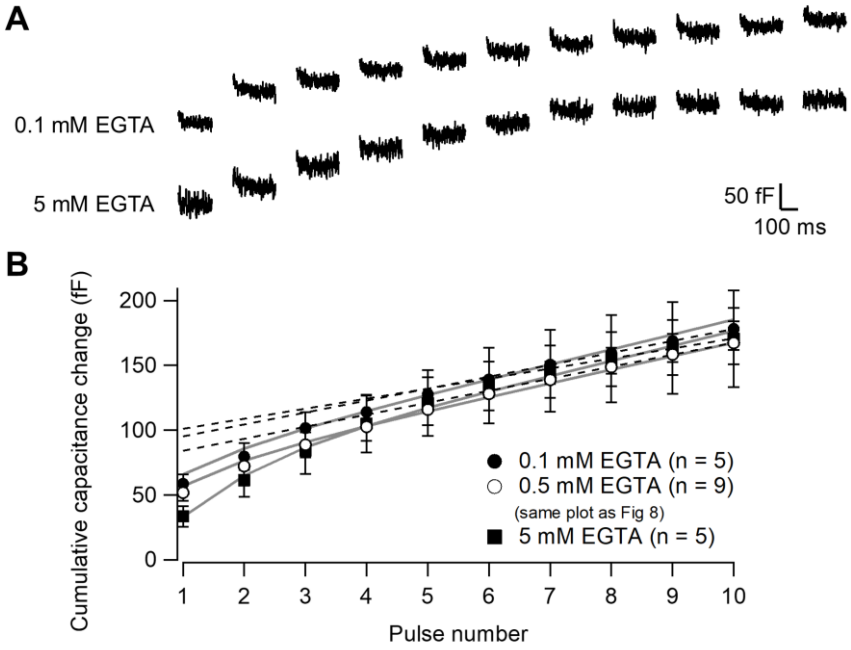

Figure 9. The repetitive stimulation experiments under different conditions of Ca^{2+} buffers suggest that synaptic vesicle replenishment is insensitive to Ca^{2+} buffers

(**A**) The stimulation protocols are the same as the one in Fig. 8 (repetitive depolarization to 0 mV). Example traces of 0.1 mM EGTA and 5 mM EGTA conditions are shown. (**B**) The cumulative capacitance jumps are plotted against the stimulus number. Filled circles, open circles, and filled squares represent the data from 0.1 mM EGTA, 0.5 mM EGTA, and 5 mM EGTA, respectively. Dotted lines show the extrapolation of the line fit to the later part of the train (last 3 responses) to the y-intercept. Gray lines show the simulation of the serial pool model.

2.3.4. Kinetics of endocytosis at the hippocampal mossy fiber terminal.

To examine whether endocytosis at the mossy fiber terminal has similar properties to that at other central synapses, I measured the kinetics of endocytosis at the hippocampal mossy fiber terminal using capacitance measurements. The presynaptic patch pipette contained 0.5 mM EGTA in Figure 10. Figure 10A shows the time course of capacitance decrease in response to a 20, 50 and 100 ms pulse (to 0 mV). For shorter pulses, it is technically difficult to achieve measurable endocytosis under our conditions because capacitance jumps are small (< 10 fF) and noise, as well as baseline drift,

prevents accurate measurement of endocytosis. Therefore, I have not examined the pulse below 20 ms. The capacitance decay was slow and had a time constant of 25-60 s (40 ± 8.5 s) when fitted by a single exponential. By varying the pulse duration, I could plot the time constant of capacitance decay over the amplitudes of capacitance jumps (Fig. 10B). The relationship was shallowly dependent on the stimulus duration. The slow time course of endocytosis also suggests that vesicle replenishment to the fully depleted RRP is not mediated by rapid synaptic vesicle cycling.

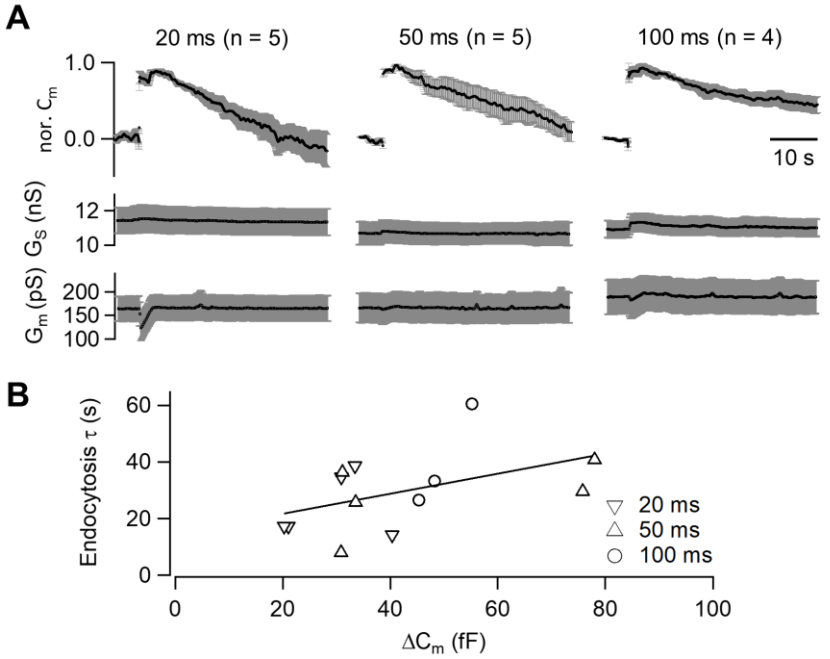

Figure 10. The time course of synaptic vesicle endocytosis at the mossy fiber terminal

(**A**) Capacitance changes elicited by depolarization to 0 mV for 20, 50, and 100 ms are shown. The patch pipette contained 0.5 mM EGTA. The data are normalized to the peak value and are averaged among cells. Average series conductance (G_s) and membrane conductance (G_m) are also shown. Error bars indicate SEM. (**B**) The capacitance decay was fitted by a single exponential, to measure the rate of synaptic vesicle endocytosis. The exponential time constants are plotted against the capacitance jumps. The line fit was $\tau = 14.6 + 0.35\ \Delta C_m$.

To examine Ca^{2+}-dependence of the endocytosis (Hosoi et al., 2009; Wu et al., 2009), I measured endocytosis under a higher EGTA concentration (5 mM) (Fig. 11A). When a 100 ms pulse

was applied, the capacitance decay was not slowed and had a time constant of tens of seconds. It is possible that higher EGTA reduces the amounts of exocytosis, thereby reducing the demand of endocytosis and accelerating the endocytosis (which may counteract with the effect of EGTA). However, the endocytotic decay time constants were not different when the amplitudes of capacitance jumps were similar between two conditions. Specifically, the 5 mM EGTA data obtained by a 100 ms pulse were similar to the 0.5 mM EGTA data obtained by a 20 ms pulse, suggesting that endocytosis was not sensitive to Ca^{2+} buffers ($p > 0.05$ for both capacitance jumps and the time constants of endocytosis) (Fig. 11B). Instead of EGTA, I also examined the effects of 1 mM BAPTA, which is assumed to have strong effects if endocytosis is Ca^{2+} sensitive and the site for endocytosis is located close to Ca^{2+} channels (Hosoi et al., 2009; Wu et al., 2009). Again, the capacitance decay was similar to the condition of 0.5 mM EGTA ($p > 0.05$ for both capacitance jumps and the time constants of endocytosis) (Fig. 11). In summary, the time course of endocytosis was insensitive to Ca^{2+} buffers under our experimental condition.

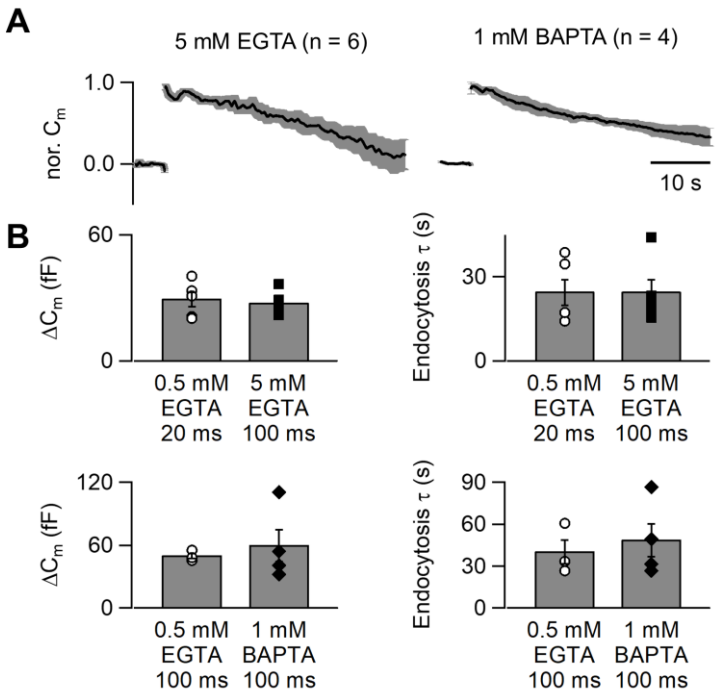

Figure 11. Synaptic vesicle endocytosis under high concentrations of Ca^{2+} buffers

(**A**) The patch pipette contained 5 mM EGTA *(left)* or 1 mM BAPTA *(right)*. The terminal was depolarized to 0 mV for 100 ms and the normalized capacitance traces are shown. Error bars indicate SEM. (**B**) *(top)* The capacitance jumps *(left)* and the decay time constants of capacitance decay *(right)* in response to a 20 ms pulse in 0.5 mM EGTA and a 100 ms pulse in 5 mM EGTA. *(bottom)* The capacitance jumps *(left)* and the time constants of capacitance decay *(right)* in response to a 100 ms pulse in 0.5 mM EGTA and 1 mM BAPTA. Capacitance jumps were similar under these conditions. Error bars indicate SEM.

2.4. Discussion

I have measured the Ca^{2+}-dependent kinetics of exo- and endocytosis at hippocampal mossy fiber terminals at room temperature. The kinetics of exocytosis was sensitive to Ca^{2+} buffers such as EGTA and BAPTA, consistent with the idea of a loose coupling between Ca^{2+} channels and synaptic vesicles. By contrast, vesicle replenishment to the RRP and endocytosis were insensitive to Ca^{2+} buffers, suggesting that they were insensitive to Ca^{2+}. At hippocampal mossy fiber terminals, there were two vesicle pools with a similar size: RRP and RP, and RP fed the vesicles to the RRP during

the stimulus train. By using the model simulation, I suggested that vesicle dynamics can be explained by two vesicle pools and Ca^{2+}-independence of synaptic vesicle replenishment.

2.4.1. Kinetics of exocytosis and its sensitivity to Ca^{2+} buffers.

The RRP and the RP have a size of ~60 fF in the present study, which corresponds to ~600 vesicles each. Midorikawa and Sakaba (2017) also suggested a similar size of the RRP. In the study by Hallermann et al. (2003), the RRP size was larger (~100 fF) although it was variable, and our data fell into their range. Hallermann et al. (2003) fitted the time course of capacitance increases with a dual exponential and the amplitude weighted time constant of release was 20 ms, which was faster than the value in the present study (30-40 ms). Hallermann et al. (2003) had a lower series resistance and this is probably why they observed a much faster Ca^{2+} current activation (Li et al., 2007). Therefore, voltage clamp in our condition must be slower, which explains the slow kinetics of Ca^{2+} currents and release in the present study. On the other hand, when series resistance is too low, run-down of exocytosis due to whole-cell dialysis becomes problematic. Therefore, I intentionally used higher access resistance to enable the assessment of synaptic vesicle replenishment.

At the calyx of Held, there are two components of release: the fast-releasing pool (FRP) (release time constant of a few ms) and the slow-releasing pool (SRP) (release time constant of 20-30 ms; Sakaba & Neher, 2001). The FRP and the SRP at the calyx may be similar to the RRP and the RP at mossy fibers, respectively. However, the overall time courses of the two components are much

slower. The properties of the SRP at the calyx are probably rather similar to those of the RRP at the mossy fibers. Previous studies have shown that the release probability in response to an action potential is estimated to be higher than that expected from the RRP size estimated in the present study (Chamberland et al., 2014; Vyleta & Jonas, 2014). The FRP, which is relevant for an action potential-evoked release, exists, although the size must be much smaller than the RRP and hidden in the large RRP. In other words, the RRP size estimate (600-700 vesicles) is potentially not physiological as a result of the artificial nature of a single long depolarizing pulse (100 ms). Indeed, Vyleta and Jonas (2014) estimated that vesicle pool size relevant for action potential-evoked release was ~50 vesicles using action potential trains in intact terminals (cell-attached recordings). Mossy fiber terminals contain ~25 AZs (Rollenhagen et al., 2007), which means ~2 vesicles per AZ are relevant for action potential-evoked release and 20-30 vesicles are released during the depolarizing pulse.

The RP at mossy fibers may be similar to recycling pool of vesicles (von Gersdorff & Matthews, 1997; Rizzoli & Betz, 2005; Qiu et al., 2015), which are not ready for rapid transmitter release at the onset of stimulation and are converted to the RRP during stimulation. The serial pool model is consistent with this idea. Morphologically, the number of vesicles within the AZs and < 60 nm from the plasma membrane is ~900, which is similar to the number of RRP + RP (Rollenhagen et al., 2007). Recent studies have suggested that docked vesicles, which are located very close to the plasma membrane (< 30 nm), are readily-releasable (Imig et al., 2014; Chang et al., 2018; Neher & Brose, 2018). The RRP may represent the vesicles that are primed and located < 30 nm from the

plasma membrane, and the RP may represent the vesicles that are slightly away from the plasma membrane. I have shown that the time course of exocytosis, but not the size of the RRP, was highly sensitive to Ca^{2+} buffer EGTA. This is consistent with the results of the study by Vyleta and Jonas (2014) showing the relatively high sensitivity of an action potential-evoked transmitter release to EGTA. BAPTA is saturated at a 100 ms pulse condition, also consistent with the studies by Vyleta and Jonas (2014) and Blatow et al. (2003), indicating that buffer saturation could happen around the transmitter release sites. Although multiple mechanisms, including residual Ca^{2+} (Katz & Miledi, 1968), Ca^{2+} sensors for facilitation (Jackman et al., 2016) and broadening of action potential waveforms (Geiger & Jonas, 2000), may contribute to facilitation during repetitive stimulation of action potentials, local buffer saturation around the release sites (Rozov et al., 2001; Blatowet al., 2003; Felmy et al., 2003; Vyleta & Jonas, 2014) may be responsible for facilitation under some conditions.

2.4.2. Synaptic vesicle replenishment at the mossy fiber terminal.

I have shown that synaptic vesicle replenishment to the RRP has a time constant of 1 s. The rate constant is faster than that of retinal bipolar cells (von Gersdorff & Matthews, 1997) but is slower than that of cerebellar mossy fiber terminals (Saviane & Silver, 2006; Ritzau-Jost et al., 2014). At the calyx of Held synapses, the replenishment has rapid and slow components with time constants of hundreds of milliseconds and several seconds, respectively (Wu & Borst, 1999; Sakaba & Neher,

2001). In the dual pulse experiments, recovery from depletion could be fitted by a single exponential. However, at an interval of 10 s, the capacitance jumps were not fully recovered (Fig. 7). It is highly probable that a slow recovery component exists.

I have also shown that rapid synaptic vesicle replenishment is insensitive to Ca^{2+} buffers, suggesting that the replenishment is relatively independent of Ca^{2+} influx. This is similar to the recent findings at cerebellar mossy fiber terminals (Ritzau-Jost et al., 2018). The calyx of Held terminals have Ca^{2+}-sensitive and -insensitive components of recovery (Wu & Borst, 1999; Sakaba & Neher, 2001; Lipstein et al., 2013). For the FRP, which is responsible for action potential-evoked release, the release time constant is 2-3 ms and vesicle replenishment is Ca^{2+}-sensitive. The SRP at the calyx of Held has the release time constant of 20-30 ms and is loosely coupled to Ca^{2+} channels (Sakaba & Neher, 2001; Wadel et al., 2007) and its recovery from depletion is fast and Ca^{2+}-independent. Given Ca^{2+}-independent recovery and the slow release kinetics, the characteristics of the SRP at the calyx are similar to those of RRP at mossy fiber terminals (Sakaba, 2018), except that, in the present study, I found a much slower recruitment speed of this pool of vesicles in the hippocampus compared to the calyx.

The model simulation suggested that the serial model fitted the data quite effectively by assuming two vesicle pools and Ca^{2+}-independent vesicle recruitment (Figs 8 and 9). At the calyx of Held, such a serial model holds for the relationship between the FRP and the SRP (Wu & Borst, 1999; Lee et al., 2012). Lee et al. (2012) have suggested a rapid transition from the SRP to the FRP within

tens of milliseconds. Accordingly, I should observe a very rapid recovery in the dual pulse experiments. At the shortest interval, the response recovered to 20-30%, which may indicate such a rapid transition. I should note that the data could be fitted by alternative models. For example, the modified serial model, which assumes that vesicles fuse from both the RRP and the RP (Wu & Borst, 1999; Ritzau-Jost et al., 2018), could fit the data. Similarly, the parallel model, which assumes parallel vesicle recruitment to the RRP and the RP (and release from both pools), could fit the data (data not shown). Nevertheless, all of the models assume two vesicle pools and Ca^{2+}-independent vesicle recruitment. I should also note that the models cannot explain why the slow phase of the RRP recovery exists and why the fraction of recovery was smaller under 0.1 mM EGTA. Other factors have to be postulated, such as activity dependent slowing of recovery (Hosoi et al., 2009; Guo et al., 2015) and consumption of vesicles through asynchronous release in low Ca^{2+} buffering conditions (Otsu et al., 2004). Further experimental analysis would be required to construct the complete vesicle pool model.

2.4.3. Synaptic vesicle endocytosis at mossy fiber terminals.

At mossy fiber terminals, the time constant of endocytosis at room temperature was slower (40 ± 8.5 s) than that of previous study (~20 s: Delvendahl et al., (2016)). In my study, endocytosis was evoked by prolonged depolarization (100 ms), and previous study used a train of short, AP-like pulses (1 ms, 10 stimuli). Endocytosis has a limited capacity and the time course of endocytosis becomes slower as the stimulus gets stronger (Delvendahl et al., 2016). In contrast to the endocytosis

at room temperature, Delvendahl et al. (2016) have observed faster endocytosis at physiological temperature. It remains to be determined whether endocytosis at physiological temperature is operated by different mechanisms such as ultrafast endocytosis (Watanabe et al., 2013) or the same mechanism (Balaji & Ryan, 2007). Fast endocytosis at rat hippocampal mossy fibers is clathrin-independent and dynamin-dependent and only appears to occur at physiological temperature (Delvendahl et al., 2016). At the mouse calyx of Held, fast endocytosis also occurs at high temperatures (Renden & von Gersdorff, 2007). Thus, the conclusion here that endocytosis is Ca^{2+}-independent (or insensitive to buffering) is thus limited to the slow mode of endocytosis, which is the dominant mode at room temperature. A recent study showed that different time scales of endocytosis could be mediated by the same clathrin-independent mechanism (Soykan et al., 2017). Nevertheless, because the time course of endocytosis is slow, newly-endocytosed vesicles probably do not participate in rapid synaptic vesicle replenishment.

In addition, I have found that endocytosis was insensitive to Ca^{2+} buffers, suggesting that endocytosis is independent of Ca^{2+}. This is in contrast to the calyx of Held, where endocytosis is sensitive to BAPTA and, to a lesser extent, EGTA (Hosoi et al., 2009; Wu et al., 2009; Yamashita et al., 2010). In ribbon synapses, Ca^{2+} accelerates (Beutner et al., 2001; Neves et al., 2001; Hull & von Gersdorff, 2004) or inhibits endocytosis (von Gersdorff & Matthews, 1994), depending on cell types and stimulus conditions. It is possible that the modes of endocytosis and its Ca^{2+} sensitivity are distinct among synapse types.

I should also note that endocytosis in the present study has been measured by whole-cell recordings. The whole-cell rundown of endocytosis can be rapid in some nerve terminals and the baseline C_m can also drift during the recordings (Hull & von Gersdorff, 2004). In addition, soluble proteins including Ca^{2+} buffers may be washed out. Therefore, the slow endocytosis measured in the present study could be a result of whole-cell dialysis and the use of the perforated patch-clamp could be a better way of measuring endocytosis.

In conclusion, I have dissected vesicle pools at the mossy fiber terminal and showed that synaptic vesicle replenishment and endocytosis are relatively Ca^{2+}-independent. Further analysis will be required to reveal the underlying molecular/cellular mechanisms of synaptic vesicle cycling at this terminal.

I investigated the kinetics and Ca^{2+}-dependence of synaptic vesicle cycle at rat hippocampal mossy fiber terminals in this chapter. At hippocampal mossy fiber terminals, the coupling distance between Ca^{2+} channels and synaptic vesicles is loose, and characteristics of synaptic vesicle cycle were different from those of other synapses with tight Ca^{2+} channel-synaptic vesicle coupling. It is assumed that such differences make synaptic diversity. At presynaptic terminals, AZ-scaffold proteins regulate the vesicle fusion machinery by controlling Ca^{2+} channel localization and vesicle docking/priming. It is likely that the molecular compositions and functions of AZ proteins may differ between the synapses with loose and tight Ca^{2+} channel-vesicle coupling. To get insights into molecular physiology of the coupling, in the next chapter, I examined the role of one AZ protein,

RIM-BP2, at hippocampal mossy fiber terminals.

3. RIM-BP2 is required for rapid neurotransmitter release through regulation of Ca^{2+} channel clustering at hippocampal mossy fiber terminals.

3.1. Introduction

Rab3-interacting molecule-binding proteins (RIM-BPs) represent one principal, conserved family of AZ proteins and bind to RIMs and Ca^{2+} channels (Wang et al., 2000; Hibino et al., 2002). RIM-BP family includes RIM-BP1, RIM-BP2, and RIM-BP3 in mammals, but RIM-BP3 expression is low in the nervous system (Mittelstaedt & Schoch, 2007). *Drosophila* neuromuscular junctions (NMJs) have a single RIM-BP gene, and loss of RIM-BP decreases Ca^{2+} channel density and reduces release probability (Liu et al., 2011). Moreover, RIM-BP is necessary for tight coupling of synaptic vesicles to Ca^{2+} channels and replenishment of high release probability vesicles at *Drosophila* NMJs (Liu et al., 2011; Müller et al., 2015; Petzoldt et al., 2020). In mammalian synapses, the observations from KO mice are diverse. In RIM-BP1,2 DKO mice, the coupling between Ca^{2+} channels and synaptic vesicles became loose, and action potential-evoked neurotransmitter release was reduced at the calyx of Held synapse (Acuna et al., 2015). At hippocampal CA3-CA1 synapses, RIM-BP2 deletion alters Ca^{2+} channel localization at the AZs without altering total Ca^{2+} influx. Besides, RIM-BP1,2 DKO has no additional effect, indicating that RIM-BP2 dominates the function of RIM-BP isoforms (Grauel et al., 2016). KO of RIM-BP2 loosened the Ca^{2+} channel-synaptic vesicle coupling,

thereby decreasing rapid release. Thus, tight coupling between Ca^{2+} channels and vesicles is crucial for rapid and efficient transmitter release (Wadel et al., 2007).

In contrast to calyx of Held synapses and hippocampal CA3-CA1 synapses, hippocampal mossy fiber-CA3 synapses are characterized by low release probability (Vyleta & Jonas, 2014). At hippocampal mossy fiber synapses, time-gated STED (gSTED) imaging, detecting the fluorescence signal after hundreds of picoseconds from excitation and getting improved resolution, suggested that RIM-BP2 deletion results in alternation of the Munc13-1 cluster number and distribution. In addition, RIM-BP2 deletion decreased the number of docked vesicles (Brockmann et al., 2019). However, the underlying mechanisms remain unclear. The reduction of fEPSPs could be due to one or more of the functional roles of AZ scaffolds: insufficient vesicle priming, looser coupling between Ca^{2+} channels and vesicles, or reduction of Ca^{2+} influx into the terminal. It is difficult to dissect a specific role of RIM-BP2, because Brockman et al. mainly used fEPSP measurements. Also, direct and quantitative measurements of exocytosis in RIM-BP2 KO terminals have not been performed so far because of technical difficulty.

To investigate RIM-BP2 functions in synaptic transmission quantitatively, I performed whole-cell patch-clamp recordings from WT and RIM-BP2 KO hippocampal mossy fiber boutons. I measured the size of the RRP of synaptic vesicles, Ca^{2+} influx, Ca^{2+} sensitivity of vesicle fusion, and the sensitivity of release to an intracellular Ca^{2+} buffer. From electrophysiological recordings, I show that Ca^{2+} current amplitudes are reduced in RIM-BP2 KO terminals, and that the reduction of Ca^{2+}

currents is the dominant factor for that of transmitter release. Using STED imaging, I find the densities of P/Q-type Ca^{2+} channels in terminals to be reduced in RIM-BP2 KO. I suggest that RIM-BP2 regulates the number of P/Q-type Ca^{2+} channels at the AZ and is critical for rapid transmitter release at hippocampal mossy fiber terminals.

3.2. Materials and Methods

3.2.1. Slice preparation

All animal experiments were conducted in accordance with the guidelines of the Physiological Society of Japan and were approved by Doshisha University Animal Experiment Committee (A22063, D22063).

I used male and female C57BL/6 mice (postnatal days 35-40). The constitutive RIM-BP2 KO mice were kindly provided by Stephan Sigrist, Dietmar Schmitz and Christian Rosenmund (Grauel et al., 2016). WT and RIM-BP2 KO mice were deeply anesthetized with isoflurane and decapitated. Their brains were quickly removed and chilled in sherbet-like cutting solution containing (in mM): 87 NaCl, 75 sucrose, 25 $NaHCO_3$, 1.25 NaH_2PO_4, 2.5 KCl, 10 glucose, 0.5 $CaCl_2$ and 7 $MgCl_2$ bubbled with 95% O_2 and 5% CO_2 (Hallermann et al., 2003). Hippocampal slices (300 μm thick) were prepared from brains using a vibratome (VT1200S, Leica) in ice-cold cutting solution. After slicing, slices were incubated in cutting solution at 37°C for 30 min, and subsequently kept at room temperature (22-25°C) up to 4 h.

3.2.2. Whole-cell recordings

Electrophysiological recordings were performed in a recording chamber filled with the extracellular solution containing (in mM): 125 NaCl, 2.5 KCl, 25 glucose, 25 $NaHCO_3$, 1.25 NaH_2PO_4, 0.4 ascorbic acid, 3 myo-inositol, 2 Na-pyruvate, 2 $CaCl_2$ and 1 $MgCl_2$ saturated with 95% O_2 and 5% CO_2. In some experiments, the concentration of $CaCl_2$ was changed to 1 mM, 1.5 mM and 4 mM. For membrane capacitance measurements, 1 μM tetrodotoxin (TTX, Wako) was added to block Na^+ channels. Moreover, for recording Ca^{2+} currents, 10 mM TEA-Cl was added to block K^+ channels. Slices were visualized by an upright microscope (BX-51, Olympus). Whole-cell patch-clamp recordings were applied to hippocampal mossy fiber terminals at room temperature. The patch pipettes were filled with the intracellular solution containing (in mM): 135 Cs-gluconate, 20 TEA-Cl, 10 HEPES, 5 Na_2-phosphocreatine, 4 MgATP, 0.3 GTP and 0.5 EGTA (pH = 7.2 adjusted with CsOH). In some experiments, the concentration of EGTA was changed to 5 mM. Presynaptic patch pipettes (BF150-86-10, Sutter Instrument) had a resistance of 15-20 MΩ and series resistance (R_s) was 30-70 MΩ. R_s was compensated so that residual resistance was 30-35 MΩ. Patch-clamp recordings were performed using an EPC10/3 amplifier (HEKA) in voltage-clamp mode, controlled by Patchmaster software (HEKA). Membrane currents were low-pass filtered at 2.9 kHz and sampled at 20 kHz. Membrane capacitance measurements were performed using an EPC10/3 amplifier in the sine + DC configuration (Gillis, 2000) using Patchmaster software (HEKA). A sine wave (30 mV in amplitude, 1000 Hz in frequency) was superimposed on the holding potential of -80 mV. Data were obtained

from at least three different WT and RIM-BP2 KO terminals in each set of experiments (biological replicate).

3.2.3. Immunostaining

Brains of WT and RIM-BP2 KO mice were quickly removed and transferred to cryomold (Sakura Finetek) filled with tissue freezing medium (Leica). Brains were instantaneously frozen on aluminum block in liquid nitrogen and stored at -80°C. For cryosectioning, frozen brains were kept in cryostat (CM1860, Leica) at −18°C for 30 min. Then, 10 µm-thick sections were sliced and collected on cover glasses (Matsunami glass, 25×25 No.1). Sections were quickly fixed by dehydration with a heat blower at 50°C for 1 min, and further dehydrated in ethanol for 30 min at -25°C and in acetone for 10 min on ice. After blocking with PBS containing 0.3% Bovine serum albumin (BSA) at room temperature, sections were incubated with primary antibodies diluted in PBS containing 0.3% BSA: anti-VGLUT1 (1:2000, Synaptic Systems, guinea pig polyclonal, RRID:AB_887878), anti-PSD-95 (1:50, NeuroMab, Mouse monoclonal IgG2a, clone K28/43, TC Supernatant, RRID:AB_2877189), anti-Munc13-1 (1:1000, Mouse monoclonal IgG1, clone 11B-10G, Sakamoto et al., 2018), and anti-Cav2.1 (1:400, Synaptic Systems, rabbit polyclonal, RRID:AB_2619841) or anti-Cav2.2 (1:400, Synaptic Systems, Mouse monoclonal IgG2b, clone 163E3, RRID:AB_2619843) or anti-RIM-BP2 (1:200, Mouse monoclonal IgG2b, clone 8-4G, Sakamoto et al., 2022) for 3 hours at room temperature. Afterwards, sections were washed and

incubated with fluorescence dye labeled secondary antibodies: DyLight 405 Anti-Guinea Pig IgG (Jackson ImmunoResearch, RRID:AB_2340470), Alexa Fluor 488 (Thermo Fisher Scientific) labeled Anti-Mouse IgG2a (Jackson ImmunoResearch, RRID:AB_2338462), STAR635P (Abberior) labeled Anti-Mouse IgG1 (Jackson ImmunoResearch, RRID:AB_2338461), and Alexa Fluor 594 (Thermo Fisher Scientific) labeled Anti-Rabbit IgG (Jackson ImmunoResearch, RRID:AB_2340585) or Anti-Mouse IgG2b (Jackson ImmunoResearch, RRID:AB_2338463) for 1 hour at room temperature (Table 1). Sections were post-fixed with 4% PFA in PBS and washed with PBS. Sections were mounted on coverslips using Prolong Glass Antifade Mountant (Thermo Fisher Scientific). The same number of sections were obtained from WT and RIM-BP2 KO brains and processed in parallel at the same experimental day (biological replicate).

Table 1. List of antibodies used in this study

Primary antibodies	Host	Clone	Dilution	Source	RRID
Anti-VGLUT1	Guinea Pig	polyclonal	1:2000	Synaptic Systems	AB_887878
Anti-PSD-95	Mouse	monoclonal IgG2a, clone K28/43, TC Supermatant	1:50	NeuroMab	AB_2877189
Anti-Munc13-1	Mouse	monoclonal IgG1, clone 11B-10G	1:1000	Sakamoto et al., 2018	
Anti-Cav2.1	Rabbit	polyclonal	1:400	Synaptic Systems	AB_2619841
Anti-Cav2.2	Mouse	monoclonal IgG2b, clone 163E3	1:400	Synaptic Systems	AB_2619843
Anti-RIM-BP2	Mouse	monoclonal IgG2b, clone 8-4G	1:200	Sakamoto et al., 2022	

Secondary antibodies	Host	Label	Dilution	Source	RRID
DyLight 405 Anti-Guinea Pig IgG	Donkey			Jackson ImmunoResearch	AB_2340470
Alexa 488 Anti-Mouse IgG2a	Goat			Jackson ImmunoResearch	AB_2338462
Anti-Mouse IgG1	Goat	STAR635P (Abberior)		Jackson ImmunoResearch	AB_2338461
Anti-Rabbit IgG	Donkey	Alexa 594 (Thermo Fisher Scientific)		Jackson ImmunoResearch	AB_2340585
Anti-Mouse IgG2b	Goat	Alexa 594 (Thermo Fisher Scientific)		Jackson ImmunoResearch	AB_2338463

3.2.4. STED imaging

STED imaging was performed using TCS SP8 STED 3x microscope (Leica) equipped with a 405 nm diode laser, a pulsed white light laser (WLL), a continuous 592 nm STED laser for alignment, a pulsed 775 nm STED laser, HyD detectors, and a 100× oil-immersion objective lens (NA = 1.4). STED microscopy provided a resolution of ~40 nm (x, y) and ~250 nm (z). STED images were acquired using the Leica LAS-X software with an image format of 1024×1024 pixels, 16-bit sampling, 8-line accumulations, and 11.36-zoom factor, yielding a pixel size of 10 nm. HyD detectors were

configured to counting mode with a gating from 0.5 to 6.5 nanosecond. A 405 nm diode laser was used to excite DyLight405. Alexa488, Alexa594, and STAR635P were excited using WLL at 488 nm, 561 nm, and 633 nm, respectively. The 775 nm STED laser power was set to 75% and 100% of maximum power for depletion of STAR635P and Alexa594, respectively, and delay time was set to 300 picoseconds. STED imaging was performed on thin sections obtained from four different WT and RIM-BP2 KO mice (biological replicate). Images were acquired three times from each section (technical replicate).

3.2.5. Analysis

For electrophysiological experiments, the data were analyzed by Igor Pro (WaveMetrics) or Excel (Microsoft Corp). To determine the time constant of release, an exponential fit was applied. Values are given as mean ± SEM, and n indicates the number of recorded terminals. Statistical method of sample size determination was not done, but our sample sizes are similar to those of previous studies (Hallermann et al., 2003; Midorikawa & Sakaba, 2017).

For STED imaging, data were analyzed using custom-designed programs in Mathematica (Wolfram), values were processed by Igor Pro (WaveMetrics), and pictures were created with ImageJ (NIH). To determine the area of AZs, image masks were generated from STED images of Munc13-1 by unsharp masking and image binarization. Only AZs that show co-localization with VGLUT1 and PSD-95 immunofluorescence signals were included in the analysis. To confine the analysis to the

large mossy fiber boutons, AZs in presynaptic terminals of small VGLUT1-positive area were excluded. Then, the background subtracted integral of signal intensity of Cav2.1 or Cav2.2 was quantified using the image masks of AZs. The background signal intensity was estimated from non-AZ area in the same STED images. For quantification of Cav2.1 clusters in the AZs, STED images of Cav2.1 were deconvolved using a gaussian kernel with a radius of 40 nm. Image masks of each Ca^{2+} channel were generated from deconvolved STED images by unsharp masking and image binarization. Then, the total signal intensity, the size, and the number of Cav2.1 clusters at the AZs were quantified using the image masks of Cav2.1 clusters. Values are given as mean ± SEM, and n indicates the number of animals. Statistical method of sample size determination was not done, but our sample sizes are similar to those of previous studies (Brockmann et al., 2019).

Statistical analysis was done in MATLAB (The MathWorks). To consider the data variability among terminals, Wilcoxon rank sum test was used for significance test of two groups. Significance level was set at $\alpha = 0.05$, and p values were described in the main text or figure legends.

3.3. Results

3.3.1. RIM-BP2 KO reduces synaptic vesicle release and calcium currents at hippocampal mossy fiber boutons.

To investigate the roles of RIM-BP2 in synaptic transmission, I examined the kinetics of exocytosis and Ca^{2+} influx in WT and RIM-BP2 KO synapses. I applied whole-cell patch-clamp

recordings and capacitance measurements to hippocampal mossy fiber terminals in acute slices from WT and RIM-BP2 KO mice, in order to measure Ca^{2+} currents and exocytosis directly. The patch pipette contained Cs^{+}-based internal solution and 0.5 mM EGTA to isolate Ca^{2+} currents (Midorikawa & Sakaba, 2017). The external solution contained 1 μM TTX to block Na^{+} currents. Membrane capacitance was measured by applying a sinusoidal wave (1000 Hz, ±30 mV in amplitudes, Lindau & Neher, 1988). When the terminal was depolarized from -80 mV to +10 mV for 10 ms, Ca^{2+} currents and membrane capacitance were recorded as shown in Figure 12A. During the depolarizing pulse, capacitance was not measured due to large conductance changes, and the increase was used for measuring synaptic vesicle exocytosis. To determine the size of the RRP and the time course of exocytosis, I measured capacitance changes (ΔC_m) in response to various durations of depolarization. Here, the length of the depolarizing pulse was varied between 5 ms and 100 ms, and ΔC_ms were plotted against pulse duration (Fig. 12B, bottom). ΔC_m in response to a 10 ms pulse was reduced in RIM-BP2 KOs ($p = 0.0499$). ΔC_m became larger as the duration of pulse was prolonged, but the increase started to be saturated at a 100 ms pulse in WT terminals, suggesting depletion of the RRP. ΔC_m in response to a 100 ms pulse was 52 ± 9.1 fF ($n = 8$). The amplitude corresponds to the fusion of about 500-600 synaptic vesicles (Hallermann et al., 2003; Midorikawa & Sakaba, 2017). The time course of ΔC_m could be fitted by a single exponential with a time constant of 58 ± 11 ms. In RIM-BP2 KO terminals, ΔC_m in response to a 100 ms pulse was smaller (41 ± 5.9 fF, $n = 8$) than that of WT terminals, and the release time constant (64 ± 14 ms) was not significantly different from WT

terminals (Fig. 12B, bottom). I should note that the time constant is not necessarily reliable because the ΔC_m values do not reach a plateau value at 100 ms pulse in some terminals. The amplitudes of Ca^{2+} currents were smaller in RIM-BP2 KO terminals as compared to WT terminals (Fig. 12B, top). The Ca^{2+} current in response to a 100 ms pulse was reduced by ~30% in RIM-BP2 KO terminals (27 ± 3.9 pA, n = 8) compared to WT terminals (41 ± 4.3 pA, n = 8) ($p = 0.0379$). Thus, the results show that RIM-BP2 deletion reduces both neurotransmitter release and Ca^{2+} influx.

To investigate the Ca^{2+} influx in more detail, I examined the voltage dependence of Ca^{2+} currents. Ca^{2+} currents were recorded in the presence of 1 μM TTX, a Na^+ channel blocker, and 10 mM TEA, a K^+ channel blocker. Figure 12C shows voltage step protocols and representative current traces. Ca^{2+} currents were elicited by 5 ms depolarizing pulses from a holding potential of -80 mV to various potentials to obtain I-V relationships. In both genotypes, Ca^{2+} currents started to be activated at around -20 mV, and maximal amplitude was observed at ~+10 mV (Fig. 12D). There was no major difference in the voltage dependence of Ca^{2+} currents between WT and RIM-BP2 KO mice. Consistently, activation time constants of Ca^{2+} currents were similar between WT and RIM-BP2 KO, when the terminal was depolarized to +10 mV ($\tau = 1.4 \pm 0.2$ ms in WT, n = 6; $\tau = 1.3 \pm 0.2$ ms in KO, n = 4). These results suggest a reduction in the number of Ca^{2+} channels rather than changes in activation kinetics is responsible for the current decrease observed.

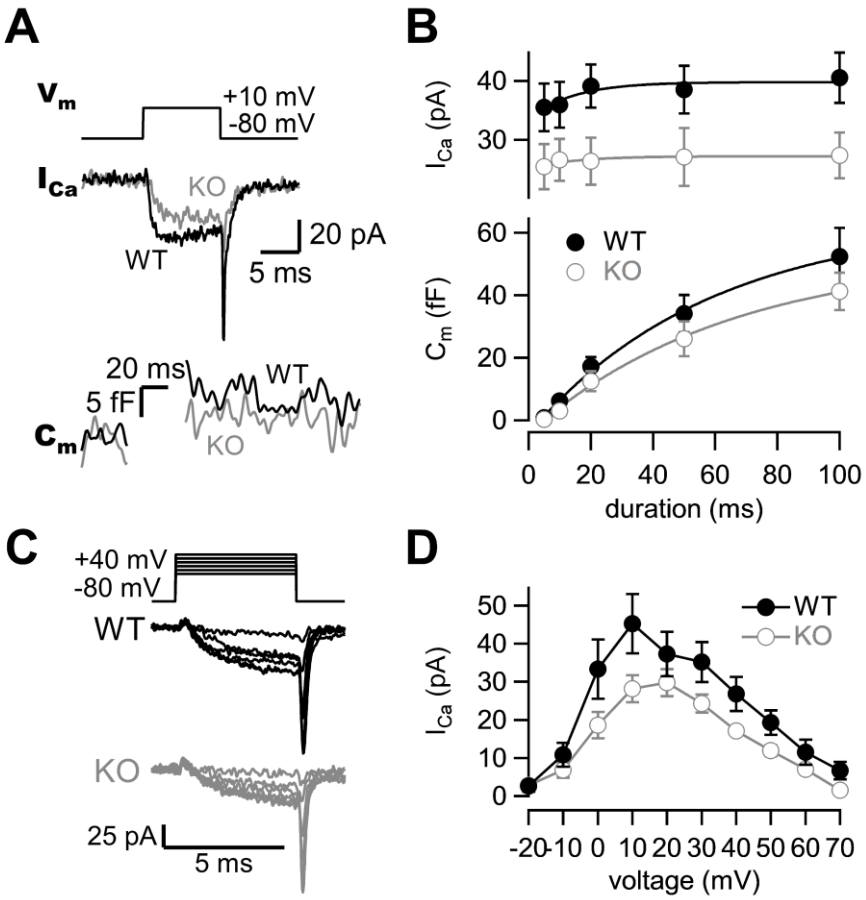

Figure 12. RIM-BP2 KO reduces calcium currents and synaptic vesicle release

(**A**) The terminal was depolarized from -80 mV to +10 mV in WT (black) and RIM-BP2 KO (gray) hippocampal mossy fiber boutons. Ca^{2+} currents (I_{Ca}) and membrane capacitance (C_m) in response to a 10 ms pulse (V_m) are shown. (**B**) *(top)* The peak Ca^{2+} currents were plotted against the pulse duration. At 10 ms, p = 0.0499 (Wilcoxon rank sum test). *(bottom)* The capacitance jumps were plotted against the pulse duration. At 20 and 100 ms, p = 0.0379 and 0.0379, respectively (Wilcoxon rank sum test). Black filled circles and gray open circles represent the data from WT (n = 8) and RIM-BP2 KO (n = 8), respectively. Each data point represents mean ± SEM. (**C**) Experimental protocol and representative traces for presynaptic Ca^{2+} current measurements in WT (black) and RIM-BP2 KO (gray) boutons. Terminals were sequentially depolarized for 5 ms with 2 ms intervals from -80 mV to +70 mV by 10 mV steps. (**D**) Current-voltage relationships of peak Ca^{2+} currents in WT (black filled circle; n = 4-6) and RIM-BP2 KO (gray open circle; n = 4-5). I_{Ca}s were elicited by 5 ms depolarizations. Each data point represents mean ± SEM.

3.3.2. High extracellular calcium concentration rescues the decrease of synaptic vesicle release in RIM-BP2 KO.

Ca^{2+} influx controls exocytosis by regulating vesicular release probability and/or the RRP size (Katz, 1969; Thanawala & Regehr, 2013). Because Ca^{2+} currents were reduced in RIM-BP2 KO mice, I tested whether the reduction of release in RIM-BP2 KO mice could be explained by that of Ca^{2+} influx or impaired synaptic vesicle docking / priming (Brockmann et al., 2017). To increase Ca^{2+} influx, I raised the extracellular Ca^{2+} concentration ($[Ca^{2+}]_{ext}$) from 2 mM to 4 mM. Ca^{2+} currents and membrane capacitances were recorded at 4 mM $[Ca^{2+}]_{ext}$, and amplitudes then plotted against pulse duration (Fig. 13A). Although Ca^{2+} current elicited by a 100 ms pulse in RIM-BP2 KO was still smaller (33 ± 2.7 pA, n = 3) than that in WT (47 ± 6.6 pA, n = 4) (Fig. 13B, top), elevated $[Ca^{2+}]_{ext}$ increased Ca^{2+} currents in both WT and RIM-BP2 KO mice. At 4 mM $[Ca^{2+}]_{ext}$, ΔC_m in response to a 100 ms pulse in RIM-BP2 KO was larger (51 ± 11 fF, n = 3) than at 2 mM $[Ca^{2+}]_{ext}$, and indeed showed a similar value in WT at 2 mM $[Ca^{2+}]_{ext}$ (Fig. 13B, bottom). At the same time, ΔC_m in WT was not altered (53 ± 3.2 fF, n = 4) at higher $[Ca^{2+}]_{ext}$, suggesting that the RRP in WT was already depleted at 2 mM $[Ca^{2+}]_{ext}$. Also, the time course of exocytosis at 4 mM $[Ca^{2+}]_{ext}$ in RIM-BP2 KO was similar to that of WT at 2 mM $[Ca^{2+}]_{ext}$, as the time courses were superimposable in Fig. 13B. These results suggest that a decrease in neurotransmitter release in RIM-BP2 KO could be rescued by an increase in Ca^{2+} influx, the most easily explained by a reduction of Ca^{2+} channel number.

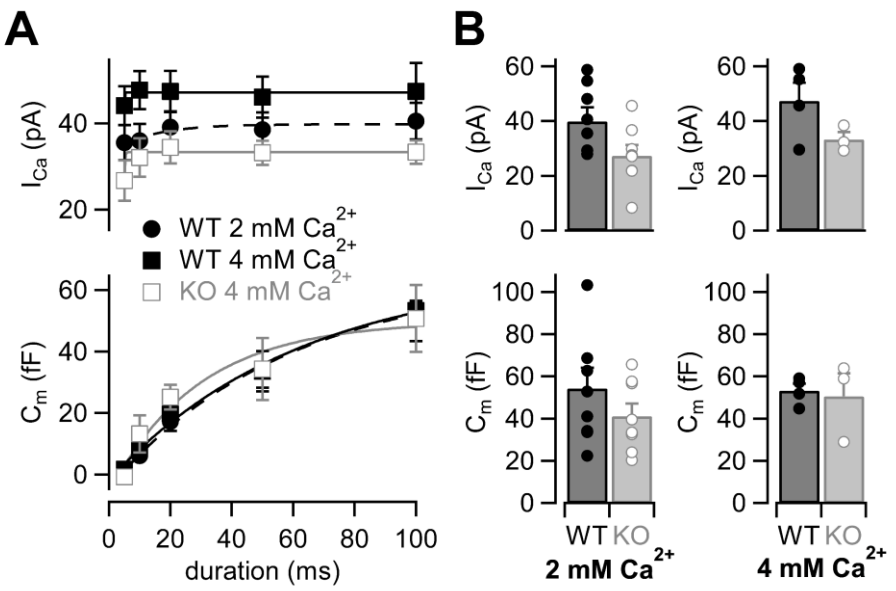

Figure 13. High extracellular calcium concentration rescues the decrease of synaptic vesicle release, but does not affect the RRP size

(**A**) *(top)* The I_{Ca}s were plotted against the pulse duration in 4 mM $[Ca^{2+}]_{ext}$. *(bottom)* The C_ms were plotted against the pulse duration in 4 mM $[Ca^{2+}]_{ext}$. Black filled squares and gray open squares represent the data from WT (n = 4-6) and RIM-BP2 KO (n = 3-4), respectively. For comparison, the WT data in 2mM $[Ca^{2+}]_{ext}$ are superimposed (black filled circle; n = 8) (the same data set as Fig. 12B). Each data point represents mean ± SEM. (**B**) Average I_{Ca}s *(top)* and C_ms *(bottom)* in response to a 100 ms pulse in WT (black bars) and RIM-BP2 KO (gray bars) terminals. Extracellular Ca^{2+} concentration was 2 mM *(left)* or 4 mM *(right)*. Error bars show SEM. Circles indicate individual values.

3.3.3. Decreased Calcium currents are mainly responsible for reduced release in RIM-BP2 KO.

In order to further address whether the observed reduction of presynaptic Ca^{2+} influx was responsible for the compromised release of RIM-BP2 KO mice, I adjusted Ca^{2+} current amplitudes of WT to that of RIM-BP2 KO by lowering $[Ca^{2+}]_{ext}$. The amplitudes of Ca^{2+} currents and capacitance jumps were plotted against pulse duration (Fig. 14A). At 1 mM $[Ca^{2+}]_{ext}$, Ca^{2+} currents and ΔC_m were smaller than those of RIM-BP2 KO at 2 mM $[Ca^{2+}]_{ext}$. At 1.5 mM $[Ca^{2+}]_{ext}$, Ca^{2+} currents became comparable to those of RIM-BP2 KO at 2 mM $[Ca^{2+}]_{ext}$. Here, the ΔC_m evoked by a 100 ms pulse (43

± 6.7 fF, n = 5) was comparable between WT and RIM-BP2 KO (Fig. 14A). The average time course of capacitance increase of WT at 1.5 mM $[Ca^{2+}]_{ext}$ was similar to that of RIM-BP2 KO at 2 mM $[Ca^{2+}]_{ext}$. Therefore, by reducing Ca^{2+} currents, WT data could reproduce the release time course of RIM-BP2 KO. In Figure 14B, ΔC_m in response to a 100 ms pulse at various $[Ca^{2+}]_{ext}$s were plotted against the peak Ca^{2+} current amplitudes. The relationship could be fitted by a Hill plot with n = 3 in WT (Schneggenburger et al., 1999). Consistently, when capacitance jumps elicited by various pulse durations are plotted against total Ca^{2+} influx (Fig. 15), the RIM-BP2 KO data were superimposed on the WT data, indicating that Ca^{2+}-sensitivity for release was not altered and that the reduction of Ca^{2+} currents determine the reduced release in RIM-BP2 KO. In Figure 14C, relative amplitudes of Ca^{2+} currents and capacitance in response to a 100 ms pulse are plotted. The RIM-BP2 KO data were superimposed on the WT data. These results confirmed that synaptic vesicles have similar sensitivity to Ca^{2+} influx in both genotypes.

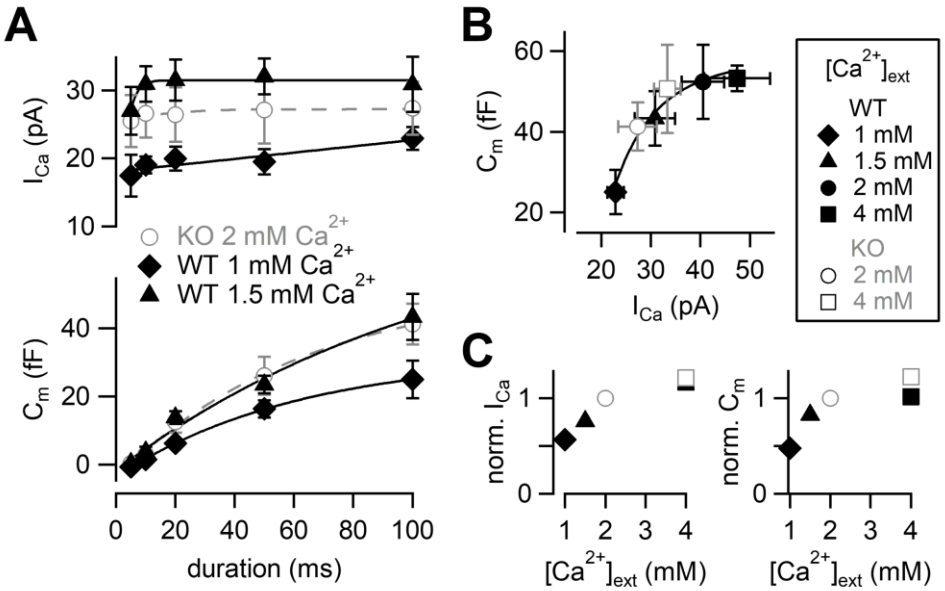

Figure 14. Calcium-dependence of the release kinetics and the RRP size

(**A**) *(top)* The relationship between peak Ca^{2+} currents and pulse durations at different $[Ca^{2+}]_{ext}$s. *(bottom)* The

relationship between capacitance jumps and pulse durations at different $[Ca^{2+}]_{ext}$s. Gray open circles, black diamonds and black triangles represent the data from RIM-BP2 KO at 2 mM $[Ca^{2+}]_{ext}$ (n = 8) (the same data set as Fig. 12B), WT at 1 mM $[Ca^{2+}]_{ext}$ (n = 3-5) and WT at 1.5 mM $[Ca^{2+}]_{ext}$ (n = 5-7), respectively. Each data point represents mean ± SEM. (**B**) Capacitance jumps at various $[Ca^{2+}]_{ext}$s are plotted against calcium current amplitudes. Pulses were 100 ms depolarization from -80 mV to +10 mV. Each data point represents mean ± SEM. Data points were fitted with a Hill equation with n = 3. (**C**) *(left)* Average I_{Ca}s at indicated $[Ca^{2+}]_{ext}$s were normalized to the response at 2 mM $[Ca^{2+}]_{ext}$ in each genotype. *(right)* Average C_ms at indicated $[Ca^{2+}]_{ext}$s were normalized to the 2 mM $[Ca^{2+}]_{ext}$ response in each genotype.

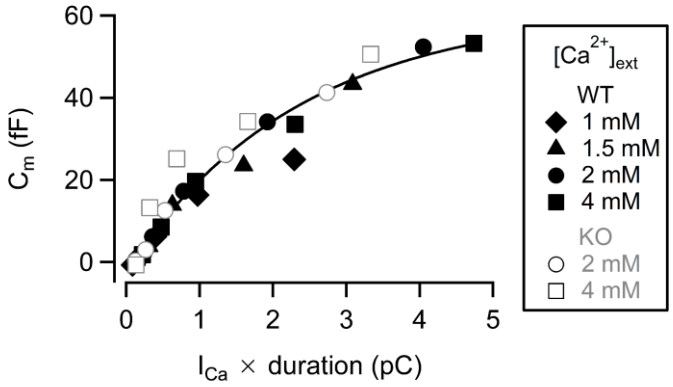

Figure 15. The relationship between synaptic vesicle release and total Ca^{2+} charge

Capacitance jumps elicited by various pulse durations are plotted against total Ca^{2+} charge. The total Ca^{2+} charge is calculated by multiplying a peak Ca^{2+} current amplitude by pulse duration. Each symbol represents a data point obtained from WT (black filled symbols) and RIM-BP2 KO (gray open symbols) mice at various $[Ca^{2+}]_{ext}$. Data points were fitted by a single exponential function.

3.3.4. High EGTA experiments suggest unaltered coupling between calcium channels and synaptic vesicles.

Previous studies have used Ca^{2+} chelator such as EGTA to examine the sensitivity of release to intracellular Ca^{2+} buffers (Adler et al., 1991; Borst & Sakmann, 1996; Vyleta & Jonas, 2014). When the physical coupling between Ca^{2+} channels and synaptic vesicles is tight, EGTA (slow Ca^{2+} chelator) has less effect on release probability, but EGTA is effective when the coupling is loose. Previous

experiments have suggested that RIM-BPs regulate the channel-vesicle coupling at the calyx of Held (Acuna et al., 2015). If this observation also applies to the mossy fiber synapse, EGTA sensitivity of release should be higher in RIM-BP2 KO terminals. To investigate the coupling at mossy fiber boutons in RIM-BP2 KO, I changed the concentration of EGTA in the patch pipette. In the presence of 5 mM EGTA, I depolarized the terminal from -80 mV to +10 mV for 5 ms and recorded Ca^{2+} currents and membrane capacitance (Fig. 16A). Ca^{2+} currents and ΔC_ms were plotted against pulse duration (Fig. 16B). In both WT and RIM-BP2 KO mice, ΔC_ms were reduced under 5 mM EGTA compared with the control condition of 0.5 mM EGTA. I compared the effect of EGTA on average amplitudes of peak Ca^{2+} currents in response to a 20 ms pulse (Fig. 16D). Interestingly, Ca^{2+} current amplitudes were ~1.5 times larger at 5 mM EGTA (53 ± 12 pA, n = 5) than at 0.5 mM EGTA (39 ± 3.7 pA, n = 8) in WT, though the data scattered under 5 mM EGTA condition and there was no statistically significant difference (p = 0.524). In RIM-BP2 KO, I did not observe such an increase. EGTA might inhibit Ca^{2+} channel inactivation in WT (von Gersdorff & Matthews, 1996). In RIM-BP2 KO, Ca^{2+} channel inactivation was not observed under 5 mM EGTA, possibly because of reduction of Ca^{2+} influx or else stronger inactivation of P/Q-type Ca^{2+} channels over other types (Lee et al., 2000). In Figure 16C, I compared the effect of EGTA on the ΔC_m in response to a 20 ms pulse. In both genotypes, ΔC_m values were inhibited by 5 mM EGTA, and the inhibition was larger in RIM-BP2 KO.

Ca^{2+} current amplitudes in RIM-B2 KO are smaller than in WT (Fig. 16B). It is possible that

strong effect of high EGTA on release maybe due to reduced Ca^{2+} currents in RIM-BP2 KO. Therefore, I changed $[Ca^{2+}]_{ext}$ from 2 mM to 1 mM and adjusted Ca^{2+} current amplitudes of WT to the RIM-BP2 KO level. The capacitance increase and the amplitudes of Ca^{2+} currents became similar to those of RIM-BP2 KO (Fig. 16C and Fig. 16D). These results indicate that WT and RIM-BP2 KO terminals have similar sensitivity of neurotransmitter release to EGTA. Thus, it is unlikely that changes in the coupling distance are responsible for the reduced exocytosis of the mutants.

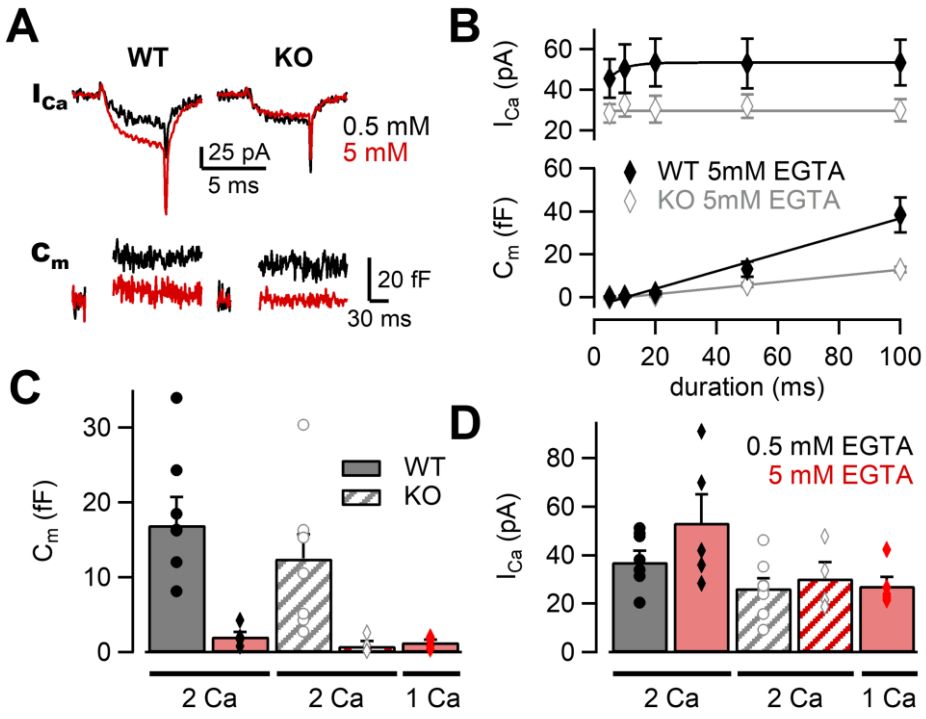

Figure 16. The effects of high EGTA on calcium currents and synaptic vesicle exocytosis

(**A**) Example traces in response to a 5 ms depolarizing pulse to +10 mV in WT *(left)* and RIM-BP2 KO *(right)* boutons. Ca^{2+} current (I_{Ca}) and membrane capacitance (C_m) recorded with 0.5 mM EGTA (black) or 5 mM EGTA (red) in the patch pipette are shown. (**B**) The I_{Ca}s *(top)* and C_ms *(bottom)* are plotted against the pulse duration. The patch pipette contained 5 mM EGTA. Black filled diamonds and gray open diamonds represent the data from WT (n = 4-5) and RIM-BP2 KO (n = 4), respectively. Each data point indicates mean ± SEM. (**C, D**) Average C_ms (**C**) and I_{Ca}s (**D**) elicited by a 20 ms pulse in WT (filled bars) and RIM-BP2 KO (hatched bars). The extracellular Ca^{2+} concentration was 1 mM or 2 mM. The intracellular solution contained either 0.5 mM EGTA (black) or 5 mM EGTA (red). Error bars show SEM. Circles and diamonds indicate individual values.

3.3.5. STED microscopy reveals that RIM-BP2 KO reduces the density of P/Q-type Ca^{2+} channels.

Our electrophysiological data suggest that RIM-BP2 may regulate the density of Ca^{2+} channels, or possibly Ca^{2+} channel properties. In order to directly study the Ca^{2+} channel density at the AZ, I performed STED microscopy analysis of Ca^{2+} channels in WT and RIM-BP2 KO hippocampal mossy fiber terminals. I here focused on P/Q-type and N-type Ca^{2+} channels because both Ca^{2+} channel types are relevant for transmitter release at this synapse (Castillo et al., 1994; Pelkey et al., 2006; Li et al., 2007). I performed immunohistochemistry on thin brain cryosections from WT and RIM-BP2 KO mice. STED microscopy confirmed complete loss of RIM-BP2 proteins in KO terminals (Fig. 17). I then immunohistochemically labeled the α-subunit of either P/Q-type Ca^{2+} channel (Cav2.1) or N-type Ca^{2+} channel (Cav2.2) and Munc13-1 (AZ/release site marker, Böhme et al., 2016; Sakamoto et al., 2018) with VGLUT1 (presynaptic marker) and PSD-95 (postsynaptic marker) (Fig. 18A, Fig. 18B and Fig. 19A). In the stratum lucidum of the hippocampal CA3 region, mossy fibers form large synapses containing multiple and clustered AZs on CA3 pyramidal cells, and also small synapses containing a single AZ on interneurons (Acsády et al., 1998; Rollenhagen et al., 2007). Thus, I identified AZs using Munc13-1 STED images and quantified the signal intensity of Cav2.1 or Cav2.2 only at AZs clustered in large VGLUT1 positive terminals in the CA3 stratum lucidum, allowing us to confine the analysis to large mossy fiber terminals innervating onto CA3 pyramidal cells. The total signal intensity of Cav2.1 at the AZ was 22% lower in RIM-BP2

KO mice (n = 4 animals) than in WT mice (n = 4 animals) (p = 0.0286) (Fig. 18C). These data are consistent with the reduction of Ca^{2+} currents in RIM-BP2 KO mice. In contrast to Cav2.1, the total signal intensity of Cav2.2 and Munc13-1 did not significantly differ between WT and RIM-BP2 KOs (p = 0.3143 and p = 0.0831) (Fig. 19B). Furthermore, I found that the number of Cav2.1 clusters within the AZ identified by STED deconvolution analysis was not altered (2.5 ± 0.11 in WT, n = 4 animals; 2.3 ± 0.02 in KO, n = 4 animals) (p = 0.114). These data suggest that RIM-BP2 KO reduces the number of P/Q-type Ca^{2+} channels per cluster. To optically estimate physical distances between Ca^{2+} channels and release sites, I next analyzed the nearest neighboring distance between Cav2.1 and Munc13-1 clusters. These distances were unchanged (61 ± 1.4 nm in WT, n = 4 animals; 64 ± 1.3 nm in KO, n = 4 animals) (p = 0.200) (Fig. 18D), consistent with the similar sensitivity of release to EGTA between WT and RIM-BP2 KO mice. From these results, I conclude that decreased Ca^{2+} influx in RIM-BP2 KO hippocampal mossy fiber terminals is caused by reduction in the density of P/Q-type Ca^{2+} channels at the AZ.

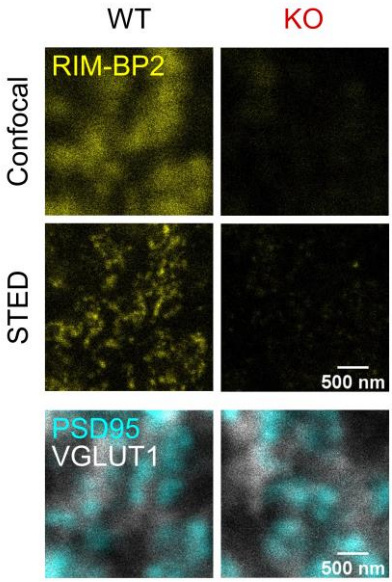

Figure 17. STED microscopy confirmed loss of RIM-BP2 proteins in KO terminals

Confocal *(top)* and STED *(middle)* images of RIM-BP2 (yellow) in WT *(left)* and RIM-BP2 KO *(right)* CA3 stratum lucidum. Hippocampal mossy fiber terminals are identified by PSD95 (cyan) and VGLUT1 (white) *(bottom)*. (Scale bar: 500 nm.) The *bottom* images show the same region as *top* and *middle*.

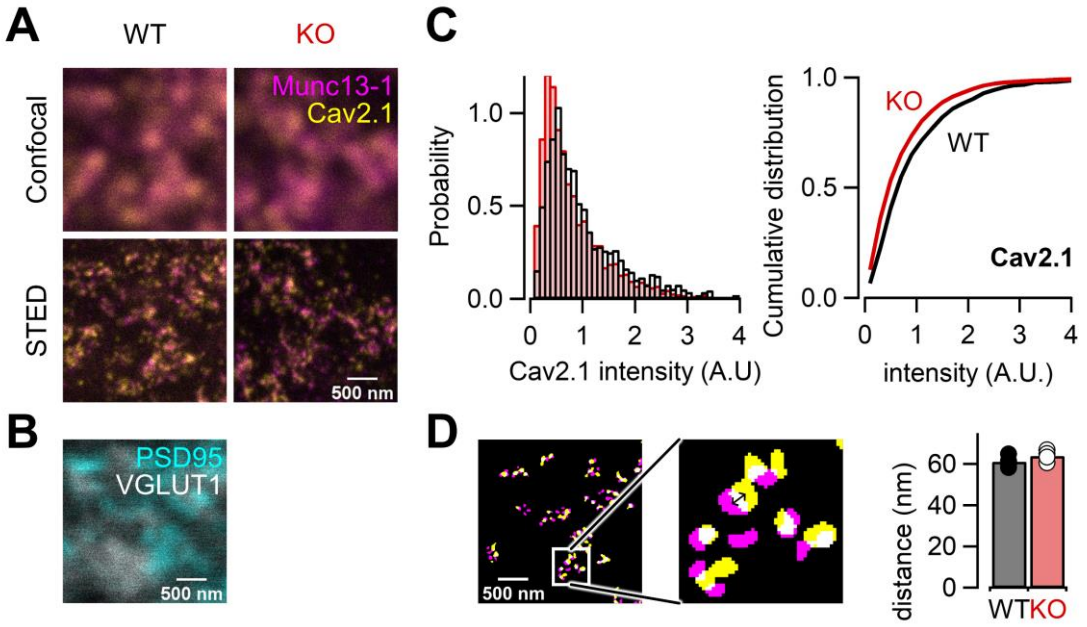

Figure 18. RIM-BP2 deletion alters the density of Cav2.1 clusters within the AZ

(**A**) Confocal *(top)* and STED *(bottom)* images of Munc13-1 (magenta) and Cav2.1 (yellow) clusters at CA3 stratum lucidum of WT *(left)* and RIM-BP2 KO *(right)* mice. (Scale bar: 500 nm.) (**B**) Confocal images of PSD95 (cyan) and VGLUT1 (white) to identify glutamatergic synapses in CA3 stratum lucidum: mossy fiber-CA3 synapses. (Scale bar: 500 nm.) The image is taken from same region shown in (**A**), *(left)*. (**C**) Histograms *(top)* and cumulative distribution plots *(bottom)* of the total signal intensity of Cav2.1 at AZs in WT (black)

and RIM-BP2 KO (red) mice. (**D**) *(left)* Cav2.1 (yellow) and Munc13-1 (magenta) clusters at AZs of hippocampal mossy fiber terminals. The image is taken from same region shown in (**A**), *(left)*. (Scale bar: 500 nm.) *(middle)* Expanded image of *(left)*, white box (500 nm square). The arrow shows a distance between Cav2.1 and Munc13-1 cluster (arrow length: 43 nm). *(right)* The average nearest neighbor distance between Cav2.1 and Munc13-1 clusters in WT (black; n = 4 animals) and RIM-BP2 KO (red; n = 4 animals) mice. Several hundreds of AZs per image were analyzed. Data show the average value of distance per animal and error bars represent SEM. Each data point indicates individual values.

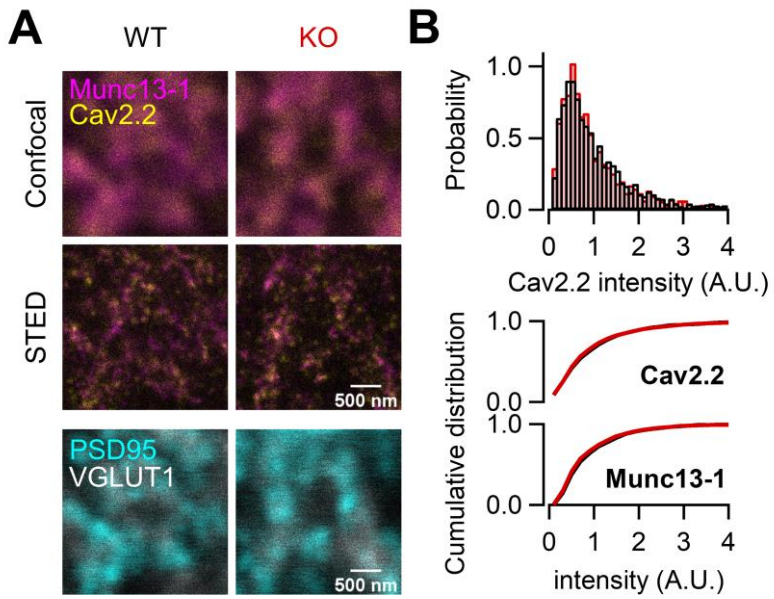

Figure 19. STED imaging of Cav2.2 at hippocampal mossy fiber terminals

(**A**) Confocal *(top)* and STED *(middle)* images of Munc13-1 (magenta) and Cav2.2 (yellow) clusters in WT *(left)* and RIM-BP2 KO *(right)* mice. Confocal images of PSD95 (cyan) and VGLUT1 (white) in the same region as *top* and *middle* are also shown *(bottom)*. (Scale bar: 500 nm.) (**B**) Histograms *(top)* and cumulative distribution plots *(bottom)* of the total signal intensity of Cav2.2, and Munc13-1 at AZs in WT (black) and RIM-BP2 KO (red) mice.

3.4. Discussion

Accumulation of Ca^{2+} channels at the AZ, and efficient vesicle docking and priming are essential factors for fast synaptic vesicle exocytosis. AZ proteins are critical for fast synchronous release and synaptic diversity. RIM-BPs have been implicated in recruitment of Ca^{2+} channels to the

AZ (Kaeser et al., 2011; Liu et al., 2011) by interacting with RIMs and Ca^{2+} channels (Wang et al., 2000; Hibino et al., 2002). In addition, RIM-BPs, like RIM1/2, recruit Munc-13 and accelerate synaptic vesicle priming (Brockmann et al., 2020). It is unclear whether RIM-BP2 affects either Ca^{2+} channel recruitment or vesicle priming or both. Furthermore, it is unclear whether the RIM-BP2 function differs among synapse types.

At murine central synapses, RIM-BPs deficient synapses demonstrate overall a rather mild decrease in the amounts of transmitter release (Acuna et al., 2015; Grauel et al., 2016; Luo et al., 2017; Krinner et al., 2017; Brockmann et al., 2019; Butola et al., 2021). Most studies so far have been focused on synapses with high release probability (phasic synapses) such as the calyx of Held and CA3-CA1 synapses. This said, at mossy fiber-CA3 synapses, KO of RIM-BPs has a strong influence on synaptic transmission (Brockmann et al., 2019). Notably, at mossy fiber-CA3 synapses, release probability is relatively low (tonic synapses). It was unknown whether the reduction of transmitter release at RIM-BP2 KO mossy fiber synapses is due to impaired Ca^{2+} channel recruitment, compromised vesicle docking or priming. Using STED microscopy, Brockmann et al. (2019) suggested that the physical recruitment of Munc13-1 might be an important function of RIM-BP2, though functional demonstration had been lacking.

By using direct presynaptic patch-clamp recordings, I here observed a decrease of Ca^{2+} current amplitudes (~30%) in RIM-BP2 KO mice (Fig. 12). As the rates of exocytosis steeply depend on Ca^{2+} influx (Dodge & Rahamimoff, 1967), the reduced Ca^{2+} influx is likely sufficient to explain

the slowed release time course at RIM-BP2 KO mossy fiber synapses. Moreover, STED microscopy supported decreased density of P/Q-type Ca^{2+} channels (Cav2.1) in the mutant mossy fiber terminal. Brockmann et al. (2019) observed a reduction of Munc13-1 cluster number and docked vesicles in RIM-BP2 deficient synapses at hippocampal mossy fiber terminals. They identified the terminals by using anti-ZnT3 antibody, enriched at mossy fiber (Brockmann et al., 2019; Wenzel et al., 1997). Our STED imaging surprisingly did not detect differences in Munc13-1 cluster number at the AZ between WT and RIM-BP2 KO mice. Notably, I analyzed the number of Cav2.1, Cav2.2 and Munc13-1 clusters only within AZs showing direct co-localization with VGLUT1 and PSD-95, which mainly reflects the AZs facing CA3 pyramidal cells rather than the synapses onto interneurons (Acsády et al., 1998; Rollenhagen et al., 2007). Such a difference in areas analyzed between previous and our study might explain the difference. Still, our results do not exclude roles of RIM-BP2 in synaptic vesicle priming. I however suggest that the reduced Ca^{2+} influx might be more critical here when compared to effects of impaired vesicle priming.

Recent studies have reported that RIM-BPs deletion altered Ca^{2+} channel localization and loosened the coupling between Ca^{2+} channels and synaptic vesicles at phasic synapses (Acuna et al., 2015; Grauel et al., 2016; Butola et al., 2021). In highly contrast, the sensitivities of release to Ca^{2+} chelator EGTA were unchanged at the mossy fiber terminals between WT and RIM-BP2 KO, which was also supported by unaltered distance between Ca^{2+} channel clusters and Munc13-1 clusters in RIM-BP2 KO terminals.

At phasic synapses, deletion of RIM-BP2 affects physical distance between Ca^{2+} channels and synaptic vesicles. In contrast, at hippocampal mossy fiber terminals having low release probability (Vyleta & Jonas, 2014), RIM-BP2 KO decreased the number of P/Q-type Ca^{2+} channels, thereby reducing Ca^{2+} influx and neurotransmitter release. Thus, I hypothesize the specific molecular-architectural and biochemical contributions by RIM-BPs might be of different relevance between phasic and tonic synapses. Brockmann et al. (2020) proposed that RIM-BP2 controls Ca^{2+} channel recruitment and vesicle priming by profound interaction with RIMs and Munc13s. These results have been obtained through studying hippocampal cultures dominated by phasic synapses. It seems possible that the interaction among three protein types is tight at phasic synapses, simply because of high density of these proteins at AZs. Alternatively, one might speculate about additional proteins, different interaction surfaces taken, transsynaptic columns (Tang et al., 2016). Deletion of RIM-BP2 does not lead to loss of Ca^{2+} channels themselves and/or vesicle priming due to remaining RIMs, Munc13, and other proteins, which can regulate recruitment of Ca^{2+} channels and synaptic vesicle priming without RIM-BP2. Instead, fine-tuning of release such as synchronization is compromised. I hypothesize that AZ scaffold might be differently built, leading to different consequences when eliminating one component. Hence deletion of RIM-BP2 leads to immediate loss of Ca^{2+} channels and/or vesicle priming. This is in line with the proposal that at tonic synapses, synaptic vesicles are only loosely coupled with Ca^{2+} channels (Vyleta & Jonas, 2014) and vesicles are de-primed under resting conditions (Miki et al., 2016; Neher & Brose, 2018). Future research along this line may lead

to an understanding of how fine molecular differences in the AZ scaffolds might orchestrate synaptic diversity.

4. General discussion

This study has two topics. First, I examined the kinetics and Ca^{2+}-dependence of synaptic vesicle exocytosis and endocytosis, in order to understand the Ca^{2+} effect on synaptic vesicle dynamics. Whole-cell patch-clamp recording was applied to rat hippocampal slices, and I measured membrane capacitance and Ca^{2+} currents. By using Ca^{2+} chelators, I found that exocytosis was Ca^{2+}-dependent, whereas endocytosis and vesicle replenishment were apparently Ca^{2+}-independent. Second, I investigated the function of AZ proteins to understand the molecular mechanism of transmitter release from mossy fiber terminals. Electrophysiological recording and STED imaging were applied to hippocampal slices of WT and RIM-BP2 KO mice. In RIM-BP2 KO mossy fiber terminals, the reduction of Ca^{2+} channel number decreased Ca^{2+} influx, which in turn decreased the amounts of transmitter release. Below, I compare the characteristics of vesicle fusion and pools at hippocampal mossy fiber terminals with those at calyx of Held terminals.

At hippocampal mossy fiber terminals, the time course of vesicle fusion was slow (τ = 30-40 ms), and vesicle recruitment to the RRP was Ca^{2+}-independent. The coupling between Ca^{2+} channels and synaptic vesicles is loose (Vyleta & Jonas, 2014). The calyx of Held synapses have fast (τ = 2-3 ms) and slow (τ = 20-30 ms) releasing pools (FRP and SRP) of vesicles. Synaptic vesicles of the FRP are located close to Ca^{2+} channels and vesicles of the SRP are far away from Ca^{2+} channels (Sakaba, 2018). The vesicle replenishment to the FRP is Ca^{2+}-dependent whereas the replenishment

to the SRP is Ca^{2+}-independent (Sakaba & Neher, 2001). The RRP at mossy fiber terminals is similar to the SRP at calyx of Held synapses in terms of kinetics, the coupling between Ca^{2+} channels and vesicles and Ca^{2+}-(in)dependence of vesicle recruitment (Fig. 20A). Furthermore, at hippocampal mossy fiber terminals having low release probability, RIM-BP2 KO did not affect the coupling distance but rather decreased Ca^{2+} channel density. In contrast, at calyx of Held synapses having high release probability, RIM-BP2 KO increases the distance of Ca^{2+} channel-synaptic vesicle coupling without detectable changes in the number of Ca^{2+} channels (Acuna et al., 2015). Therefore, the calyx and mossy fiber terminals seem to construct AZ scaffolds differently (Fig. 20B).

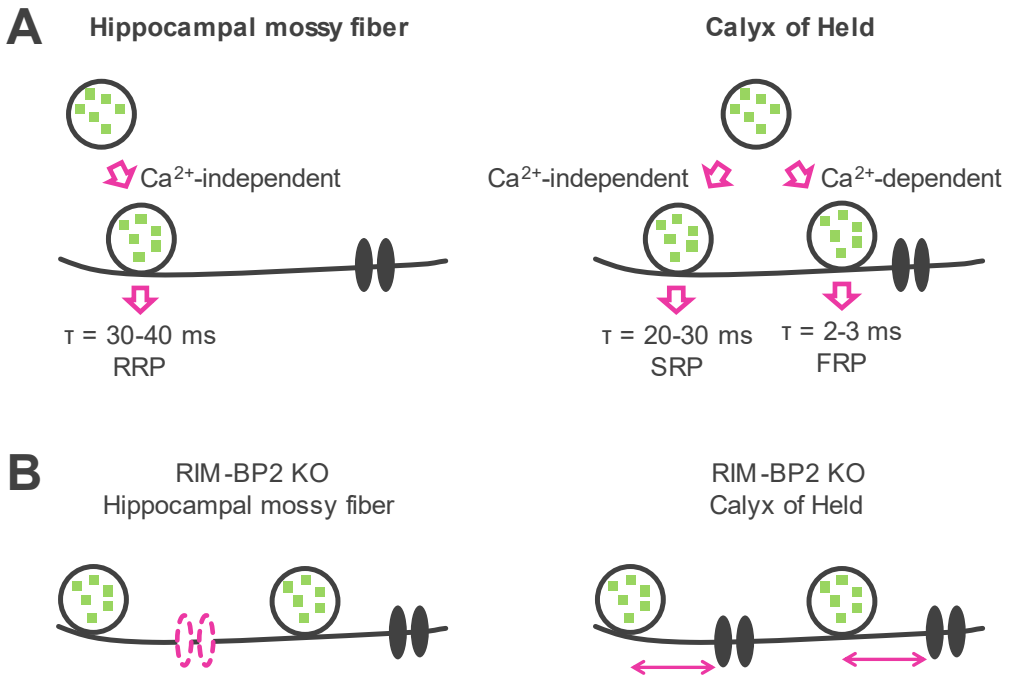

Figure 20. Comparison of hippocampal mossy fiber and the calyx of Held

(**A**) The time course of vesicle fusion and Ca^{2+}-dependence of vesicle recruitment at hippocampal mossy fiber terminals *(left)* and the calyx of Held terminals *(right)*. (**B**) RIM-BP2 deficient mice affect the number of Ca^{2+} channels at hippocampal mossy fiber terminals *(lest)* and the coupling distance between Ca^{2+} channels and synaptic vesicles at the calyx of Held terminals *(right)*.

Hippocampal mossy fiber synapses can transfer information by generating postsynaptic action potential not during low- but rather during high-frequency firing, and such a property is important for hippocampal network function such as conditional detonation. The low release probability due to the loose coupling contributes to such a high-pass filtering (Evstratova & Tóth, 2014), though other factors such as incomplete priming may contribute as well. In contrast, the calyx of Held synapse is known to generate action potentials both during low- and high-frequency signaling. The calyx of Held terminals are large, have multiple AZs with high release probability, which ensure reliable information transfer at low-frequency signaling. In addition, the calyx terminals have multiple vesicle pools and relatively rapid vesicle recruitment for sustained activity. Such properties contribute to sound localization, which requires high-frequency reliable signaling (Schneggenburger & Forsythe, 2006; Baydyuk et al., 2016). The difference in the release machinery is likely to generate unique synaptic plasticity specific to each synapse type, causing functional distinction. More experiments are needed to elucidate the molecular mechanism of synaptic transmission, to find differences in the release machinery between the synapses having low and high release probability, and to reveal the molecular mechanism of synaptic plasticity. Nevertheless, the approach used in this study, namely, combination of genetics, electrophysiology, and super-resolution optical microscopy, may lead to understanding how AZ-scaffold proteins regulate release machineries and cause synaptic plasticity and diversity.

5. References

Acsády L, Kamondi A, Sík A, Freund T, Buzsáki G. (1998). GABAergic cells are the major postsynaptic targets of mossy fibers in the rat hippocampus. *The Journal of neuroscience* **18**:3386-3403. DOI: https://doi.org/10.1523/JNEUROSCI.18-09-03386.1998, PMID: 9547246

Acuna C, Liu X, Gonzalez A, Südhof TC. (2015). RIM-BPs Mediate Tight Coupling of Action Potentials to Ca^{2+}-Triggered Neurotransmitter Release. *Neuron* **87**:1234-1247. DOI: https://doi.org/10.1016/j.neuron.2015.08.027, PMID: 26402606

Adler EM, Augustine GJ, Duffy SN, Charlton MP. (1991). Alien intracellular calcium chelators attenuate neurotransmitter release at the squid giant synapse. *The Journal of Neuroscience* **11**:1496-1507. DOI: https://doi.org/10.1523/JNEUROSCI.11-06-01496.1991, PMID: 1675264

Alabi AA, Tsien RW. (2012). Synaptic vesicle pools and dynamics. *Cold Spring Harbor perspectives in biology* **4**:a013680. DOI: https://doi.org/10.1101/cshperspect.a013680, PMID: 22745285

Augustin I, Rosenmund C, Südhof TC, Brose N. (1999). Munc13-1 is essential for fusion competence of glutamatergic synaptic vesicles. *Nature* **400**:457–461. DOI: https://doi.org/10.1038/22768, PMID: 10440375

Balaji J, Ryan TA. (2007). Single-vesicle imaging reveals that synaptic vesicle exocytosis and endocytosis are coupled by a single stochastic mode. *PNAS* **104**:20576-20581. DOI: https://doi.org/10.1073/pnas.0707574105, PMID: 18077369

Baydyuk M, Xu J, Wu LG. (2016). The calyx of Held in the auditory system: Structure, function, and development. *Hearing research* **338**:22–31. DOI: https://doi.org/10.1016/j.heares.2016.03.009, PMID: 27018297

Beutner D, Voets T, Neher E, Moser T. (2001). Calcium dependence of exocytosis and endocytosis at the cochlear inner hair cell afferent synapse. *Neuron* **29**:681-690. DOI: https://doi.org/10.1016/S0896-6273(01)00243-4, PMID: 11301027

Blatow M, Caputi A, Burnashev N, Monyer H, Rozov A. (2003). Ca^{2+} buffer saturation underlies paired pulse facilitation in calbindin-D28k-containing terminals. *Neuron* **38**:79-88. DOI:

https://doi.org/10.1016/s0896-6273(03)00196-x, PMID: 12691666

Borst JGG, Helmchen F, Sakmann B. (1995). Pre- and postsynaptic whole-cell recordings in the medial nucleus of the trapezoid body of the rat. *The Journal of physiology* **489**:825-840. DOI: https://doi.org/10.1113/jphysiol.1995.sp021095, PMID: 8788946

Borst JG, Sakmann B. (1996). Calcium influx and transmitter release in a fast CNS synapse. *Nature* **383**:431-434. DOI: https://doi.org/10.1038/383431a0, PMID: 8837774

Brockmann MM, Maglione M, Willmes CG, Stumpf A, Bouazza BA, Velasquez LM, Grauel MK, Beed P, Lehmann M, Gimber N, Schmoranzer J, Sigrist SJ, Rosenmund C, Schmitz D. (2019). RIM-BP2 primes synaptic vesicles *via* recruitment of Munc13-1 at hippocampal mossy fiber synapses. *eLife* **8**:e43243. DOI: https://doi.org/10.7554/eLife.43243, PMID: 31535974

Brockmann MM, Zarebidaki F, Camacho M, Grauel MK, Trimbuch T, Südhof TC, Rosenmund C. (2020). A Trio of Active Zone Proteins Comprised of RIM-BPs, RIMs, and Munc13s Governs Neurotransmitter Release. *Cell Reports* **32**:107960-107960. DOI: https://doi.org/10.1016/j.celrep.2020.107960, PMID: 32755572

Butola T, Alvanos T, Hintze A, Koppensteiner P, Kleindienst D, Shigemoto R, Wichmann C, Moser T. (2021). RIM-Binding Protein 2 Organizes Ca^{2+} Channel Topography and Regulates Release Probability and Vesicle Replenishment at a Fast Central Synapse. *The Journal of Neuroscience* **41**:7742-7767. DOI: https://doi.org/10.1523/JNEUROSCI.0586-21.2021, PMID: 34353898

Castillo PE, Weisskopf MG, Nicoll RA. (1994). The role of Ca^{2+} channels in hippocampal mossy fiber synaptic transmission and long-term potentiation. *Neuron* **12**:261-269. DOI: https://doi.org/10.1016/0896-6273(94)90269-0, PMID: 8110457

Chamberland S, Evstratova A, Tóth K. (2014). Interplay between synchronization of multivesicular release and recruitment of additional release sites support short-term facilitation at hippocampal mossy fiber to CA3 pyramidal cells synapses. *The Journal of neuroscience* **34**:11032-11047. DOI: https://doi.org/10.1523/JNEUROSCI.0847-14.2014, PMID: 25122902

Chang S, Trimbuch T, Rosenmund C. (2018). Synaptotagmin-1 drives synchronous Ca^{2+}-triggered fusion by C_2B-domain-mediated synaptic-vesicle-membrane attachment. *Nature neuroscience* **21**:33-40. DOI: https://doi.org/10.1038/s41593-017-0037-5, PMID: 29230057

Davydova D, Marini C, King C, Klueva J, Bischof F, Romorini S, Montenegro-Venegas C, Heine

M, Schneider R, Schröder MS, Altrock WD, Henneberger C, Rusakov DA, Gundelfinger ED, Fejtova A. (2014). Bassoon specifically controls presynaptic P/Q-type Ca^{2+} channels via RIM-binding protein. *Neuron* **82**:181–194. DOI: https://doi.org/10.1016/j.neuron.2014.02.012, PMID: 24698275

Delvendahl I, Vyleta NP, von Gersdorff H, Hallermann S. (2016). Fast, temperature-sensitive and clathrin-independent endocytosis at central synapses. *Neuron* **90**:492-498. DOI: https://doi.org/10.1016/j.neuron.2016.03.013, PMID: 27146271

Deng PY, Klyachko VA. (2011). The diverse functions of short-term plasticity components in synaptic computations. *Communicative & integrative biology* **4**:543–548. DOI: https://doi.org/10.4161/cib.4.5.15870, PMID: 22046457

Denker A, Rizzoli SO. (2010). Synaptic vesicle pools: an update. *Frontiers in synaptic neuroscience* **2**:135. DOI: https://doi.org/10.3389/fnsyn.2010.00135, PMID: 21423521

Dittman JS, Regehr WG. (1998). Calcium dependence and recovery kinetics of presynaptic depression at the climbing fiber to Purkinje cell synapse. *The Journal of neuroscience* **18**:6147-6162. DOI: https://doi.org/10.1523/JNEUROSCI.18-16-06147.1998, PMID: 9698309

Dittman JS, Kreitzer AC, Regehr WG. (2000). Interplay between facilitation, depression, and residual calcium at three presynaptic terminals. *The Journal of neuroscience* **20**:1374-1385. DOI: https://doi.org/10.1523/JNEUROSCI.20-04-01374.2000, PMID: 10662828

Dodge FA, Rahamimoff R. (1967). Co-operative action a calcium ions in transmitter release at the neuromuscular junction. *The Journal of physiology* **193**:419-432. DOI: https://doi.org/10.1113/jphysiol.1967.sp008367, PMID: 6065887

Eggermann E, Bucurenciu I, Goswami SP, Jonas P. (2011). Nanodomain coupling between Ca^{2+} channels and sensors of exocytosis at fast mammalian synapses. *Nature reviews. Neuroscience* **13**:7–21. DOI: https://doi.org/10.1038/nrn3125, PMID: 22183436

Evstratova A, Tóth K. (2014). Information processing and synaptic plasticity at hippocampal mossy fiber terminals. *Frontiers in cellular neuroscience* **8**:28. DOI: https://doi.org/10.3389/fncel.2014.00028, PMID: 24550783

Felmy F, Neher E, Schneggenburger R. (2003). Probing the intracellular calcium sensitivity of transmitter release during synaptic facilitation. *Neuron* **37**:801-811. DOI: https://doi.org/10.1016/s0896-6273(03)00085-0, PMID: 12628170

Fortune ES, Rose GJ. (2001). Short-term synaptic plasticity as a temporal filter. *Trends in neurosciences*, **24**:381–385. https://doi.org/10.1016/s0166-2236(00)01835-x, PMID: 11410267

Geiger JR, Jonas P. (2000). Dynamic control of presynaptic Ca^{2+} inflow by fast-inactivating K^{+} channels in hippocampal mossy fiber boutons. *Neuron* **28**:927-939. DOI: https://doi.org/10.1016/s0896-6273(00)00164-1, PMID: 11163277

Gillis KD. (2000). Admittance-based measurement of membrane capacitance using the EPC-9 patch-clamp amplifier. *Pflügers Archiv* **439**:655-664. DOI: https://doi.org/10.1007/s004249900173, PMID: 10764227

Grauel MK, Maglione M, Reddy-Alla S, Willmes CG, Brockmann MM, Trimbuch T, Rosenmund T, Pangalos M, Vardar G, Stumpf A, Walter AM, Rost BR, Eickholt BJ, Haucke V, Schmitz D, Sigrist SJ, Rosenmund C. 2016. RIM-binding protein 2 regulates release probability by fine-tuning calcium channel localization at murine hippocampal synapses. *PNAS* **113**:11615-11620. DOI: https://doi.org/10.1073/pnas.1605256113, PMID: 27671655

Grundy D. (2015). Principles and standards for reporting animal experiments in The Journal of Physiology and Experimental Physiology. *The Journal of physiology* **593**:2547-2549. DOI: https://doi.org/10.1113/JP270818, PMID: 26095019

Guo J, Ge JL, Hao M, Sun ZC, Wu XS, Zhu JB, Wang W, Yao PT, Lin W, Xue L. (2015). A three-pool model dissecting readily releasable pool replenishment at the calyx of Held. *Scientific reports* **5**:9517. DOI: https://doi.org/10.1038/srep09517, PMID: 25825223

Hallermann S, Pawlu C, Jonas P, Heckmann M. (2003). A large pool of releasable vesicles in a cortical glutamatergic synapse. *PNAS* **100**:8975-8980. DOI: https://doi.org/10.1073/pnas.1432836100, PMID: 12815098

Han Y, Kaeser PS, Südhof TC, Schneggenburger R. (2011). RIM determines Ca^{2+} channel density and vesicle docking at the presynaptic active zone. *Neuron* **69**:304–316. DOI: https://doi.org/10.1016/j.neuron.2010.12.014, PMID: 21262468

Haucke V, Neher E, Sigrist SJ. (2011). Protein scaffolds in the coupling of synaptic exocytosis and endocytosis. *Nature reviews. Neuroscience* **12**:127–138. DOI: https://doi.org/10.1038/nrn2948, PMID: 21304549

Henze DA, McMahon DB, Harris KM, Barrionuevo G. (2002). Giant miniature EPSCs at the hippocampal mossy fiber to CA3 pyramidal cell synapse are monoquantal. *Journal of*

neurophysiology **87**:15–29. DOI: https://doi.org/10.1152/jn.00394.2001, PMID: 11784726

He L, Wu XS, Mohan R, Wu LG. (2006). Two modes of fusion pore opening revealed by cell-attached recordings at a synapse. *Nature* **444**:102–105. DOI: https://doi.org/10.1038/nature05250, PMID: 17065984

Hibino H, Pironkova R, Onwumere O, Vologodskaia M, Hudspeth AJ, Lesage F. 2002. RIM binding proteins (RBPs) couple Rab3-interacting molecules (RIMs) to voltage-gated Ca^{2+} channels. *Neuron* **34**:411-423. DOI: https://doi.org/10.1016/s0896-6273(02)00667-0, PMID: 11988172

Hosoi N, Holt M, Sakaba T. (2009) Calcium dependence of exo- and endocytotic coupling at a glutamatergic synapse. *Neuron* **63**:216-229. DOI: https://doi.org/10.1016/j.neuron.2009.06.010,

Hull C, von Gersdorff H. (2004). Fast endocytosis is inhibited by GABA-mediated chloride influx at a presynaptic terminal. *Neuron* **44**:469-482. DOI: https://doi.org/10.1016/j.neuron.2004.10.010, PMID: 15504327

Imig C, Min SW, Krinner S, Arancillo M, Rosenmund C, Südhof TC, Rhee J, Brose N, Cooper BH. (2014). The morphological and molecular nature of synaptic vesicle priming at presynaptic active zones. *Neuron* **84**:416-431. DOI: https://doi.org/10.1016/j.neuron.2014.10.009, PMID: 25374362

Jackman SL, Turecek J, Belinsky JE, Regehr WG. (2016). The calcium sensor synaptotagmin 7 is required for synaptic facilitation. *Nature* **529**:88-91. DOI: https://doi.org/10.1038/nature16507, PMID: 26738595

Jackman SL, Regehr WG. (2017). The Mechanisms and Functions of Synaptic Facilitation. *Neuron* **94**:447-464. DOI: https://doi.org/10.1016/j.neuron.2017.02.047, PMID: 28472650

Kaeser PS, Deng L, Wang Y, Dulubova I, Liu X, Rizo J, Südhof TC. (2011). RIM proteins tether Ca^{2+} channels to presynaptic active zones via a direct PDZ-domain interaction. *Cell* **144**:282-295. DOI: https://doi.org/10.1016/j.cell.2010.12.029, PMID: 21241895

Katz B. 1969. The release of neural transmitter substances. Liverpool University Press. ISBN: 0853230609

Katz B, Miledi R. (1968). The role of calcium in neuromuscular facilitation. *The Journal of physiology* **195**:481-492. DOI: https://doi.org/10.1113/jphysiol.1968.sp008469, PMID: 4296699

Kiyonaka S, Wakamori M, Miki T, Uriu Y, Nonaka M, Bito H, Beedle AM, Mori E, Hara Y, De

Waard M, Kanagawa M, Itakura M, Takahashi M, Campbell KP, Mori Y. (2007). RIM1 confers sustained activity and neurotransmitter vesicle anchoring to presynaptic Ca^{2+} channels. *Nature neuroscience* **10**:691–701. DOI: https://doi.org/10.1038/nn1904, PMID: 17496890

Krinner S, Butola T, Jung S, Wichmann C, Moser T. (2017). RIM-Binding Protein 2 Promotes a Large Number of Cav1.3 Ca^{2+}-Channels and Contributes to Fast Synaptic Vesicle Replenishment at Hair Cell Active Zones. *Frontiers in Cellular Neuroscience* **11**:334. DOI: https://doi.org/10.3389/fncel.2017.00334, PMID: 29163046

Kushmerick C, Renden R, von Gersdorff H. (2006). Physiological temperatures reduce the rate of vesicle pool depletion and short-term depression via an acceleration of vesicle recruitment. *The Journal of neuroscience* **26**:1366-1377. DOI: https://doi.org/10.1523/JNEUROSCI.3889-05.2006, PMID: 16452660

Lawrence JJ, McBain CJ. (2003). Interneuron diversity series: containing the detonation--feedforward inhibition in the CA3 hippocampus. *Trends in neurosciences* **26**:631-640. DOI: https://doi.org/10.1016/j.tins.2003.09.007, PMID: 14585604

Lee JS, Ho WK, Lee SH. (2012). Actin-dependent rapid recruitment of reluctant synaptic vesicles into a fast-releasing vesicle pool. *PNAS* **109**:E765-E774. DOI: https://doi.org/10.1073/pnas.1114072109, PMID: 22393020

Li L, Bischofberger J, Jonas P. (2007). Differential gating and recruitment of P/Q-, N-, and R-type Ca^{2+} channels in hippocampal mossy fiber boutons. *The Journal of Neuroscience* **27**:13420-13429. DOI: https://doi.org/10.1523/JNEUROSCI.1709-07.2007, PMID: 18057200

Lindau M, Neher E. (1988). Patch-clamp techniques for time-resolved capacitance measurements in single cells. *Pflügers Archiv* **411**:137-146. DOI: https://doi.org/10.1007/BF00582306, PMID: 3357753

Lipstein N, Sakaba T, Cooper BH, Lin KH, Strenzke N, Ashery U, Rhee JS, Taschenberger H, Neher E, Brose N. (2013). Dynamic control of synaptic vesicle replenishment and short-term plasticity by Ca^{2+}-calmodulin-Munc13-1 signaling. *Neuron* **79**:82-96. DOI: https://doi.org/10.1016/j.neuron.2013.05.011, PMID: 23770256

Lipstein N, Chang S, Lin KH, López-Murcia FJ, Neher E, Taschenberger H, Brose N. (2021). Munc13-1 is a Ca^{2+}-phospholipid-dependent vesicle priming hub that shapes synaptic short-term plasticity and enables sustained neurotransmission. *Neuron* **109**:3980-4000.e7. DOI: https://doi.org/10.1016/j.neuron.2021.09.054, PMID: 34706220

Liu KS, Siebert M, Mertel S, Knoche E, Wegener S, Wichmann C, Matkovic T, Muhammad K, Depner H, Mettke C, Bückers J, Hell SW, Müller M, Davis GW, Schmitz D, Sigrist SJ. (2011). RIM-binding protein, a central part of the active zone, is essential for neurotransmitter release. *Science* **334**:1565-1569. DOI: https://doi.org/10.1126/science.1212991, PMID: 22174254

Luo F, Liu X, Südhof TC, Acuna C. (2017). Efficient stimulus-secretion coupling at ribbon synapses requires RIM-binding protein tethering of L-type Ca^{2+} channels. *PNAS* **114**:E8081-E8090. DOI: https://doi.org/10.1073/pnas.1702991114, PMID: 28874522

Mori M, Abegg MH, Gähwiler BH, Gerber U. (2004). A frequency-dependent switch from inhibition to excitation in a hippocampal unitary circuit. *Nature* **431**:453-456. DOI: https://doi.org/10.1038/nature02854, PMID: 15386013

Midorikawa M, Sakaba T. (2017). Kinetics of Releasable Synaptic Vesicles and Their Plastic Changes at Hippocampal Mossy Fiber Synapses. *Neuron* **96**:1033-1040.e3. DOI: https://doi.org/10.1016/j.neuron.2017.10.016, PMID: 29103807

Miki T, Malagon G, Pulido C, Llano I, Neher E, Marty A. (2016). Actin- and Myosin-Dependent Vesicle Loading of Presynaptic Docking Sites Prior to Exocytosis. *Neuron* **91**:808-823. DOI: https://doi.org/10.1016/j.neuron.2016.07.033, PMID: 27537485

Miki T, Nakamura Y, Malagon G, Neher E, Marty A. (2018). Two-component latency distributions indicate two-step vesicular release at simple glutamatergic synapses. *Nature communications* **9**:3943. DOI: https://doi.org/10.1038/s41467-018-06336-5, PMID: 30258069

Mittelstaedt T, Schoch S. (2007). Structure and evolution of RIM-BP genes: identification of a novel family member. *Gene* **403**:70-79. DOI: https://doi.org/10.1016/j.gene.2007.08.004, PMID: 17855024

Moser T, Beutner D. (2000). Kinetics of exocytosis and endocytosis at the cochlear inner hair cell afferent synapse of the mouse. *PNAS* **97**:883–888. DOI: https://doi.org/10.1073/pnas.97.2.883, PMID: 10639174

Mukherjee K, Yang X, Gerber SH, Kwon HB, Ho A, Castillo PE, Liu X, Südhof TC. (2010). Piccolo and bassoon maintain synaptic vesicle clustering without directly participating in vesicle exocytosis. *PNAS* **107**:6504–6509. DOI: https://doi.org/10.1073/pnas.1002307107, PMID: 20332206

Müller M, Genç Ö, Davis GW. (2015). RIM-binding protein links synaptic homeostasis to the

stabilization and replenishment of high release probability vesicles. *Neuron* **85**:1056-1069. DOI: https://doi.org/10.1016/j.neuron.2015.01.024, PMID: 25704950

Neher E. (1998). Usefulness and limitations of linear approximations to the understanding of Ca^{++} signals. *Cell Calcium* **24**:345-357. DOI: https://doi.org/10.1016/s0143-4160(98)90058-6, PMID: 10091004

Neher E. (2015). Merits and Limitations of Vesicle Pool Models in View of Heterogeneous Populations of Synaptic Vesicles. *Neuron* **87**:1131-1142. DOI: https://doi.org/10.1016/j.neuron.2015.08.038, PMID: 26402599

Neher E, Brose N. (2018). Dynamically Primed Synaptic Vesicle States: Key to Understand Synaptic Short-Term Plasticity. *Neuron* **100**:1283-1291. DOI: https://doi.org/10.1016/j.neuron.2018.11.024, PMID: 30571941

Neher E, Marty A. (1982). Discrete changes of cell membrane capacitance observed under conditions of enhanced secretion in bovine adrenal chromaffin cells. *PNAS* **79**:6712-6716. DOI: https://doi.org/10.1073/pnas.79.21.6712, PMID: 6959149

Neher E, Sakaba T. (2008). Multiple roles of calcium ions in the regulation of neurotransmitter release. *Neuron 59*:861–872. DOI: https://doi.org/10.1016/j.neuron.2008.08.019, PMID: 18817727

Neves G, Lagnado L. (1999). The kinetics of exocytosis and endocytosis in the synaptic terminal of goldfish retinal bipolar cells. *The Journal of physiology* **515**:181-202. DOI: https://doi.org/10.1111/j.1469-7793.1999.181ad.x, PMID: 9925888

Neves G, Gomis A, Lagnado L. (2001) Calcium influx selects the fast mode of endocytosis in the synaptic terminal of retinal bipolar cells. *PNAS* **98**:15282-15287. DOI: https://doi.org/10.1073/pnas.261311698, PMID: 11734626

Nicoll RA, Schmitz F. (2005). Synaptic plasticity at hippocampal mossy fibre synapses. *Nature reviews. Neuroscience* **6**:863-876. https://doi.org/10.1038/nrn1786, PMID: 16261180

Otsu Y, Shahrezaei V, Li B. Raymond LA, Delaney KR, Murphy TH. (2004). Competition between phasic and asynchronous release for recovered synaptic vesicles at developing hippocampal autaptic Synapses. *The Journal of neuroscience* **24**:420-433. DOI: https://doi.org/10.1523/JNEUROSCI.4452-03.2004, PMID: 14724240

Parsons TD, Lenzi D, Almers W, Roberts WM. (1994). Calcium-triggered exocytosis and

endocytosis in an isolated presynaptic cell: capacitance measurements in saccular hair cells. *Neuron* **13**:875–883. DOI: https://doi.org/10.1016/0896-6273(94)90253-4, PMID: 7946334

Pelkey KA, Topolnik L, Lacaille J-C, McBain CJ. (2006). Compartmentalized Ca^{2+} channel regulation at divergent mossy-fiber release sites underlies target cell-dependent plasticity. *Neuron* **52**:497-510. DOI: https://doi.org/10.1016/j.neuron.2006.08.032, PMID: 17088215

Petzoldt AG, Götz TWB, Driller JH, Lützkendorf J, Reddy-Alla S, Matkovic-Rachid T, Liu S, Knoche E, Mertel S, Ugorets V, Lehmann M, Ramesh N, Beuschel CB, Kuropka B, Freund C, Stelzl U, Loll B, Liu F, Wahl MC, Sigrist SJ. (2020). RIM-binding protein couples synaptic vesicle recruitment to release sites. *Journal of Cell Biology* **219**:e201902059. DOI: https://doi.org/10.1083/jcb.201902059, PMID: 32369542

Qiu X, Zhu Q, Sun J. (2015). Quantitative analysis of vesicle recycling at the calyx of Held synapse. *PNAS* **112**:4779-4784. DOI: https://doi.org/10.1073/pnas.1424597112, PMID: 25825725

Renden R, von Gersdorff H (2007). Synaptic vesicle endocytosis at a CNS nerve terminal: faster kinetics at physiological temperatures and increased endocytotic capacity during maturation. *Journal of neurophysiology* **98**:3349-3359. DOI: https://doi.org/10.1152/jn.00898.2007, PMID: 17942618

Ritzau-Jost A, Delvendahl I, Rings A, Byczkowicz N, Harada H, Shigemoto R, Hirrlinger J, Eilers J, Hallermann S. (2014). Ultrafast action potentials mediate kilohertz signaling at a central synapse. *Neuron* **84**:152–163. DOI: https://doi.org/10.1016/j.neuron.2014.08.036, PMID: 25220814

Ritzau-Jost A, Jablonski L, Viotti J, Lipstein N, Eilers J, Hallermann S. (2018). Apparent calcium dependence of vesicle recruitment. *The Journal of physiology* **596**:4693-4707. DOI: https://doi.org/10.1113/JP275911, PMID: 29928766

Rizzoli SO, Betz WJ. (2005). Synaptic vesicle pools. *Nature reviews. Neuroscience* **6**:57-69. DOI: https://doi.org/10.1038/nrn1583, PMID: 15611727

Rollenhagen A, Sätzler K, Rodríguez EP, Jonas P, Frotscher M, Lübke JHR. (2007). Structural determinants of transmission at large hippocampal mossy fiber synapses. *The Journal of Neuroscience* **27**:10434-10444. DOI: https://doi.org/10.1523/JNEUROSCI.1946-07.2007, PMID: 17898215

Rozov A, Burnashev N, Sakmann B, Neher E. (2001). Transmitter release modulation by intracellular Ca2+ buffers in facilitating and depressing nerve terminals of pyramidal cells in layer

2/3 of the rat neocortex indicates a target cell-specific difference in presynaptic calcium dynamics. *The Journal of physiology* **531**:807-826. DOI: https://doi.org/10.1111/j.1469-7793.2001.0807h.x, PMID: 11251060

Saheki Y, De Camilli P. (2012). Synaptic vesicle endocytosis. *Cold Spring Harbor perspectives in biology* **4**:a005645. DOI: https://doi.org/10.1101/cshperspect.a005645, PMID: 22763746

Sakaba T, Neher E. (2001). Calmodulin mediates rapid recruitment of fast-releasing synaptic vesicles at a calyx-type synapse. *Neuron* **32**:1119-1131. DOI: https://doi.org/10.1016/s0896-6273(01)00543-8, PMID: 11754842

Sakaba T. (2018). Kinetics of transmitter release at the calyx of Held synapse. *Proceedings of the Japan Academy. Series B, Physical and biological sciences* **94**:139-152. DOI: https://doi.org/10.2183/pjab.94.010, PMID: 29526973

Sakamoto H, Ariyoshi T, Kimpara N, Sugao K, Taiko I, Takikawa K, Asanuma D, Namiki S, Hirose K. (2018). Synaptic weight set by Munc13-1 supramolecular assemblies. *Nature neuroscience* **21**:41–49. DOI: https://doi.org/10.1038/s41593-017-0041-9, PMID: 29230050

Sakamoto H, Kimpara N, Namiki S, Hamada S, Ohtsuka T, Hirose K. (2022). Synapse type-specific molecular nanoconfigurations of the presynaptic active zone in the hippocampus identified by systematic nanoscopy [unpublished manuscript]. *bioRxiv* 2022.03.11.483942. DOI: https://doi.org/10.1101/2022.03.11.483942

Saviane C, Silver RA. (2006). Fast vesicle reloading and a large pool sustain high bandwidth transmission at a central synapse. *Nature* **439**:983-987. DOI: https://doi.org/10.1038/nature04509, PMID: 16496000

Schneggenburger R, Forsythe ID. (2006). The calyx of Held. *Cell and tissue research* **326**:311-337. DOI: https://doi.org/10.1007/s00441-006-0272-7, PMID: 16896951

Schneggenburger R, Meyer AC, Neher E. (1999). Released fraction and total size of a pool of immediately available transmitter quanta at a calyx synapse. *Neuron* **23**:399-409. DOI: https://doi.org/10.1016/s0896-6273(00)80789-8, PMID: 10399944

Soykan T, Kaempf N, Sakaba T, Vollweiter D, Goerdeler F, Puchkov D, Kononenko NL, Haucke V. (2017). Synaptic vesicle endocytosis occurs on multiple timescales and is mediated by formin-dependent actin assembly. *Neuron* **93**:854-866.e4. DOI: https://doi.org/10.1016/j.neuron.2017.02.011, PMID: 28231467

Stevens CF, Wesseling JF. (1998). Activity-dependent modulation of the rate at which synaptic vesicles become available to undergo exocytosis. *Neuron* **21**:415-424. DOI: https://doi.org/10.1016/s0896-6273(00)80550-4, PMID: 9728922

Sudhof TC. (2012). Calcium control of neurotransmitter release. *Cold Spring Harbor perspectives in biology* **4**:a011353. DOI: https://doi.org/10.1101/cshperspect.a011353, PMID: 22068972

Südhof TC. (2012). The presynaptic active zone. *Neuron* **75**:11-25. DOI: https://doi.org/10.1016/j.neuron.2012.06.012, PMID: 22794257

Sun JY, Wu LG. (2001). Fast kinetics of exocytosis revealed by simultaneous measurements of presynaptic capacitance and postsynaptic currents at a central synapse. *Neuron* **30**:171-182. DOI: https://doi.org/10.1016/s0896-6273(01)00271-9, PMID: 11343653

Tang AH, Chen H, Li TP, Metzbower SR, MacGillavry HD, Blanpied TA. (2016). A trans-synaptic nanocolumn aligns neurotransmitter release to receptors. *Nature* **536**:210-214. DOI: https://doi.org/10.1038/nature19058, PMID: 27462810

Taschenberger H, Leão RM, Rowland KC, Spirou GA, von Gersdorff H. (2002). Optimizing synaptic architecture and efficiency for high-frequency transmission. *Neuron* **36**:1127-1143. DOI: https://doi.org/10.1016/s0896-6273(02)01137-6, PMID: 12495627

Thanawala MS, Regehr WG. (2013). Presynaptic calcium influx controls neurotransmitter release in part by regulating the effective size of the readily releasable pool. *The Journal of Neuroscience* **33**:4625-4633. DOI: https://doi.org/10.1523/JNEUROSCI.4031-12.2013, PMID: 23486937

von Gersdorff H, Matthews G (1994). Inhibition of endocytosis by elevated internal calcium in a synaptic terminal. *Nature* **370**:652-655. DOI: https://doi.org/10.1038/370652a0, PMID: 8065451

von Gersdorff H, Matthews G. (1996). Calcium-dependent inactivation of calcium current in synaptic terminals of retinal bipolar neurons. *The Journal of Neuroscience* **16**:115-122. DOI: https://doi.org/10.1523/JNEUROSCI.16-01-00115.1996, PMID: 8613777

von Gersdorff H, Matthews G (1997). Depletion and replenishment of vesicle pools at a ribbon-type synaptic terminal. *The Journal of neuroscience* **17**:1919-1927. DOI: https://doi.org/10.1523/JNEUROS CI.17-06-01919.1997, PMID: 9045721

Vyleta NP, Jonas P. (2014). Loose coupling between Ca^{2+} channels and release sensors at a plastic hippocampal synapse. *Science* **343**:665-670. DOI: https://doi.org/10.1126/science.1244811, PMID:

24503854

Vyleta NP, Borges-Merjane C, Jonas P. (2016). Plasticity-dependent, full detonation at hippocampal mossy fiber-CA3 pyramidal neuron synapses. *eLife* **5**:e17977. DOI: https://doi.org/10.7554/eLife.17977, PMID: 27780032

Wadel K, Neher E, Sakaba T. (2007). The coupling between synaptic vesicles and Ca^{2+} channels determines fast neurotransmitter release. *Neuron* **53**:563-575. DOI: https://doi.org/10.1016/j.neuron.2007.01.021, PMID: 17296557

Wang LY, Kaczmarek LK. (1998). High-frequency firing helps replenish the readily releasable pool of synaptic vesicles. *Nature* **394**:384-388. DOI: https://doi.org/10.1038/28645, PMID: 9690475

Wang Y, Sugita S, Südhof TC. (2000). The RIM/NIM family of neuronal C2 domain proteins. Interactions with Rab3 and a new class of Src homology 3 domain proteins. *Journal of Biological Chemistry* **275**:20033-20044. DOI: https://doi.org/10.1074/jbc.M909008199, PMID: 10748113

Watanabe S, Rost BR, Camacho-Pérez M, Davis MW, Söhl-Kielczynski B, Rosenmund C, Jorgensen EM. (2013). Ultrafast endocytosis at mouse hippocampal synapses. *Nature* **504**:242-247. DOI: https://doi.org/10.1038/nature12809, PMID: 24305055

Weingarten DJ, Shrestha A, Juda-Nelson K, Kissiwaa SA, Spruston E, Jackman SL. (2022). Fast resupply of synaptic vesicles requires synaptotagmin-3. *Nature* **611**:320–325. DOI: https://doi.org/10.1038/s41586-022-05337-1, PMID: 36261524

Wenzel HJ, Cole TB, Born DE, Schwartzkroin PA, Palmiter RD. 1997. Ultrastructural localization of zinc transporter-3 (ZnT-3) to synaptic vesicle membranes within mossy fiber boutons in the hippocampus of mouse and monkey. *PNAS* **94**:12676-12681. DOI: https://doi.org/10.1073/pnas.94.23.12676, PMID: 9356509

Wölfel M, Schneggenburger R. (2003). Presynaptic capacitance measurements and Ca^{2+} uncaging reveal submillisecond exocytosis kinetics and characterize the Ca^{2+} sensitivity of vesicle pool depletion at a fast CNS synapse. *The Journal of neuroscience* **23**:7059-7068. DOI: https://doi.org/10.1523/JNEUROSCI.23-18-07059.2003, PMID: 12904466

Wu LG, Borst JGG (1999). The reduced release probability of releasable vesicles during recovery from short-term synaptic depression. *Neuron* **23**:821-832. DOI: https://doi.org/10.1016/s0896-6273(01)80039-8, PMID: 10482247

Wu XS, McNeil BD, Xu J, Fan J, Xue L, Melicoff E, Adachi R, Bai L, Wu LG. (2009). Ca^{2+} and calmodulin initiate all forms of endocytosis during depolarization at a nerve terminal. *Nature neuroscience* **12**:1003-1010. DOI: https://doi.org/10.1038/nn.2355, PMID: 19633667

Yamashita T, Eguchi K, Saitoh N, von Gersdorff H, Takahashi T. (2010). Developmental shift to a mechanism of synaptic vesicle endocytosis requiring nanodomain Ca^{2+}. *Nature neuroscience* **13**:838-844. DOI: https://doi.org/10.1038/nn.2576, PMID: 20562869

Zucker RS, Regehr WG. (2002). Short-term synaptic plasticity. *Annual review of physiology* **64**:355-405. DOI: https://doi.org/10.1146/annurev.physiol.64.092501.114547, PMID: 11826273